Masteroppgåve

NTNU
Noregs teknisk-naturvitskaplege universitet
Fakultet for naturvitenskap
Institutt for fysikk

Anna Lovise Rekdal

Radiation dose and image quality in CT

Comparison and evaluation of two different organ-based tube current modulation techniques and their impact on organ dose and image noise

Masteroppgåve i Fysikk og Matematikk
Veileder: Kathrine Røe Redalen
Juni 2019

NTNU
Kunnskap for ei betre verd

NTNU
Norwegian University of
Science and Technology

Radiation dose and image quality in CT

Comparison and evaluation of two different organ-based tube current modulation techniques and their impact on organ dose and image noise

Anna Lovise Rekdal

Master of science
Submission date: June 2019
Supervisor: Kathrine Røe Redalen, IFY
Co-supervisor: Daniel Austigard Aadnevik, Haukeland University Hospital

Norwegian University of Science and Technology
Department of Physics

Abstract

Background: Computed tomography (CT) examinations are used to diagnose a variety of disorders, and the use of CT is increasing [1, 2]. This increase has lead to a rising concern of the radiation dose the patients receive. It is important to optimise all radiologic procedures so that the patient receives a dose which is as low as reasonably achievable (the ALARA principle). It is possible to reduce the delivered dose to radiosensitive organs on the surface of the body in a CT scan by reducing the tube current when the X-ray tube passes over the organs. This is referred to as organ-based tube current modulation (OBTCM). Both Siemens and General Electric (GE) have developed OBTCM techniques called X-CARE and Organ Dose Modulation (ODM), respectively. X-CARE compensates for the dose reduction on the anterior by increasing the dose on the posterior, but ODM does not. This means that the total patient dose is the same for X-CARE as for a standard scan, while the total patient dose is reduced when ODM is used.

Aim: The aim of this thesis was to examine and compare the amount of noise and radiation dose reduction to the eye lenses and female breasts when X-CARE and ODM are used.

Materials and methods: Two different uniform phantoms were used for dose measurements and measurements of image noise. For each of the CT scanners, one of the phantoms was scanned with (1) a standard head protocol, (2) an OBTCM head protocol, (3) a standard chest protocol, and (4) an OBTCM chest protocol. The dose was measured with an ion chamber in different positions close to the surface of the phantom. The other phantom was scanned with standard and OBTCM chest scans. Noise was measured as the standard deviation of CT numbers inside circular regions of interest of different sizes. The noise was also visualised by making noise maps.

Results: X-CARE reduced the dose to the position of the eye lenses slightly more than ODM did ($-28 \pm 3\%$ versus $-18 \pm 1\%$). For X-CARE, the dose reduction to the breasts varied from 20% to over 50% depending on how centrally located the breasts are assumed to be. ODM gave a dose reduction to the breasts of around 35%, and was less dependent on breast position than X-CARE.

The measured image noise did not increase, compared to a standard scan, when X-CARE was used. For ODM, no increase in noise was measured for the head scan, and an increase of about 10% was measured for the chest scan. The noise maps show visually that X-CARE produced the same amount of noise as the standard scan, and that ODM caused a slight increase in noise for the chest scan.

Conclusion: Both OBTCM techniques gave a similar dose reduction to the positions where the eye lenses and the breasts are expected to be. The positioning of the breasts is crucial for X-CARE to work as intended. X-CARE gives no change in image noise, but increases the dose to the back of the body. No noise increase was measured in the ODM head scan, while a small increase of 10% was measured in the body scan. Radiologists are needed to evaluate if this increase is visible clinically.

Samandrag

Bakgrunn: Computertomografi (CT) -undersøkingar er eit mykje brukt vertøy i medisinsk dignostikk, og bruken aukar [1, 2]. Denne auka har først til auka uro over stråledosen pasientar blir utsett for. Det er viktig å optimalisere all radiologiske undersøkingar slik at pasienten får ei låg stråledose (ALARA-prinsippet). Det er mogleg å redusere stråledosen til stråleføLsame ytre organ ved å redusere røyrstraumen over desse organa. Dette blir kalla OBTCM ("organ-based tube current modulation"). Både Siemens og General Electric (GE) har utvikla OBTCM-teknikkar som dei kallar X-CARE og Organ Dose Modulation (ODM). X-CARE kompenserer for den reduserte dosen på framsida av pasienten ved å auke dosen på baksida, medan ODM ikkje gjer dette. Det tyder at den totale pasientdosen er lik for X-CARE som for eit standardscan, medan den totale pasientdosen blir redusert når ODM blir brukt.

Målsetting: Målet med denne avhandlinga var å undersøkje og samanlikne mengda støy og stråledosereduksjonen til augelinsene og kvinnebrysta når X-CARE og ODM blir brukt.

Materiell og metodar: To ulike uniforme fantom vart brukte til dosemålingar og måling av biletestøy. For kvar av dei to CT scannarane vart det eine fantomet scanna med (1) ein standard hovudprotokoll, (2) ein OBTCM hovudprotokoll, (3) ein standard thoraxprotokoll, og (4) ein OBTCM thoraxprotokoll. Dosen vart målt med eit ionekammer på ulike posisjonar nær overflata til fantomet. Det andre fantomet vart scanna med standard og OBTCM thoraxprotokollar. Støy vart målt som standardavviket i CT-tal innanfor sirkulære interesseområde. Støyen vart òg visualisert ved å lage støykart.

Resultat: X-CARE reduserte dosen i området der augelinsene er litt meir enn ODM ($-28 \pm 3\%$ versus $-18 \pm 1\%$). For X-CARE varierer dosereduksjonen til brysta frå 20% og opp til over 50% avhengig av kor sentralt ein antek at brysta er plassert. ODM reduserte brystdosen med rundt 35%, og var mykje mindre avhengig av brystposisjon enn X-CARE.

Den målte støyen i bileta auka ikkje, samanlikna med eit standard scan, når X-CARE vart brukt. Når ODM vart brukt vart det målt ikkje målt nokon støyauke for hovudbileta, men ei auke på omtrent 10% vart målt i thoraxbileta. Støykarta for thoraxprotokollane viser visuelt at X-CARE gir lik støy som standardscannet, og at ODM gir ei lita støyauke.

Konklusjon: Begge OBTCM-teknikkane gir liknande dosereduksjon til området der augelinsene og brysta er forventa å vere. God posisjonering av brysta er naudsynt for at X-CARE skal fungere etter planen. X-CARE gir inga endring i biletestøy, men aukar dosen til baksida av pasienten. Inga støyauke vart målt for OBM hovudprotokollen, men ei lita auke på omtrent 10% vart målt for thoraxprotokollen. Radiologvurderingar trengst for å evaluere om denne støyauka er merkbar klinisk.

Acknowledgements

I would like to express my sincere gratitude to my supervisor Daniel Aadnevik at Haukeland University Hospital (HUH). Thank you for your support and encouragement throughout the entire process, and for being so excited and involved in the project that you could rarely wait to see the results. You have been so supportive in everything from commute routes to technical explanations. Your PowerPoint slides are the best. Many thanks are also due to the rest of the team of physicists at HUH. Thank you, Kirsten Bolstad, for your endless patience and great suggestions. Thank you, Anette Guleng, for showing me just what it takes to write a Master thesis, and for all the encouraging words. Thank you Saana Jenu for lending me your desk and for taking the time to read my work even though we never met. Thank you all for all your help, and for giving me a second home in Bergen. You made me able to do this.

I would also like to thank my internal supervisor at NTNU, Kathrine Redalen, for including me in her research group, for being available, and for making sure all the formalities of my degree are in order.

I am grateful to the radiographers Vibeke Hjelle and Ørjan Kjærstad at Haraldsplass, and Eivind Nilsen at HUH for helping me with the experimental setup. I hope you will find the results interesting.

I would like to take the opportunity to thank my family, both for enabling me to start this journey of education, and to finish it. I don't know who I would be without you.

And last, but by no means least; dear Christoph, thank you for filling my days with sunshine and marzipan. Thank you for being you. You are perfect.

And thanks be to You, who is with me always.

Anna Rekdal
Trondheim, May 2019

Abbreviations

ALARA	=	As low as reasonably achievable
ATCM	=	Automatic tube current modulation
CNR	=	Contrast-to-noise ratio
CT	=	Computed tomography
CTDI	=	Computed tomography dose index
DLP	=	Dose-length product
FBP	=	Filtered back-projection
FOV	=	Field of view
GE	=	General Electric
HDS	=	Haraldsplass Diakonale sykehus
HU	=	Hounsfield units
HUH	=	Haukeland University Hospital
ICRP	=	International Commission on Radiological Protection
kV	=	Accelerating voltage
kVp	=	Kilovolt peak
LNT	=	Linear no-threshold
mAs	=	Tube current-time product
OBTCM	=	Organ-based tube current modulation
ODM	=	Organ dose modulation
PMMA	=	Polymethyl methacrylate
ROI	=	Region of interest
WL	=	Window level
WW	=	Window width

Contents

Chapter 1

Introduction

The medical field was revolutionised when doctors were able to use radiation to examine the inside of a patient's body, and X-ray imaging quickly became an indispensable tool in diagnostic medicine. X-rays are widely used in a variety of procedures, using either two-dimensional images (radiography), real-time image guidance during non-invasive surgery and the creation of slices and three-dimensional images of the body using computed tomography (CT). While the information obtained by exposing a patient to radiation often will be life-saving, the radiation will also expose the patient to a possible risk. Ionising radiation, like X-rays, may damage the cells in the body. This can lead to acute damage, like eye damage and hair loss, as well as possible long-term carcinogenic effects. The information obtained from a radiologic procedure must therefore outweigh the risk involved, and each procedure should be optimised to provide the necessary diagnostic information at the lowest possible dose. Compared to X-ray radiography, a CT scan will use a higher radiation dose, and thus involves a higher risk for radiation-induced effects to occur [1].

Some organs in the body are more radiosensitive than others. These will often be given special consideration when a patient is exposed to radiation during treatment and examinations. In CT examinations the surface of the patient receives a larger amount of dose than the centre. Radiosensitive organs positioned on the exterior of the body, like the eye lenses and female breasts, will receive a higher radiation dose than radiosensitive internal organs. Often these surface organs are within the area of examination, but are not themselves objects of examination. One way to protect them is to avoid direct irradiation of the area. However, this is not always possible, and in these cases a physical shield of bismuth is sometimes used. Bismuth shields have the disadvantage of producing artifacts (errors) in the image [3]. An alternative approach is to reduce the intensity of the X-ray beam as it passes over these organs.

Siemens and General Electric (GE) have developed CT protocols aiming to reduce the radiation dose to the eye lenses and breasts according to this principle. Siemens' solution is called X-CARE, and in addition to reducing the intensity of the beam when it passes over these organs, it increases the intensity in the remaining part of the rotation in order to maintain the image quality. GE's solution Organ Dose Modulation (ODM) does not compensate for the reduced intensity during parts of the rotation, but allows a reduction of image quality in order to reduce the patient dose.

In this thesis, the X-CARE and ODM techniques will be compared and evaluated in terms of how the different techniques affect image noise and radiation dose to the eye lenses and breasts,

relative to standard CT scans. Additionally, the influence of different patient sizes on the two techniques will be considered.

Chapter 2

Theory

In a CT scanner, the patient is irradiated from several angles, spread out over a full rotation of 360°, producing image "slices" which together provide three-dimensional image data. Because of this, the procedure is called 'computed tomography', from the Greek word 'tomos', meaning 'slice' or 'section' [4]. CT is an imaging modality which uses the attenuation of X-rays in the body to create images of the inside of the body. Highly attenuating tissues, such as bone, absorb more of the incoming X-rays, while less attenuating tissues, such as the lungs, let more of the radiation pass through. In traditional projection radiography, all structures in the irradiated area are projected onto one image, meaning that they are all shown on top of each other, without any information about their relative depths. This also means that structures can be hidden from view because they are "behind" other structures. This problem is avoided in CT images.

CT technology was greatly developed in the 1960s and 1970s, and the first clinical CT scans were published by Sir Godfrey N. Hounsfield and Dr. James Ambrose in 1972 [5]. In 1979 Hounsfield and Allan M. Cormack were jointly awarded the Nobel price in Physiology or Medicine for the development of computer assisted tomography. The use of CT had radically changed the field of medical imaging, and made diagnostic medicine more accurate. This is especially the case for head examinations, where the surrounding skull makes traditional planar radiography of the brain almost useless [5]. Today, CT scanners are in use all over the world, and are used as a standard diagnostic tool.

CT examinations have become an indispensable diagnostic tool, but also give the patient a relatively high radiation dose compared to other imaging modalities. Of the medical imaging examinations in Norway on 2008, CT scans accounted for only 21% of the number of examinations, but for as much as 80% of the collective dose given (compared to conventional X-ray, ultrasound and MRI) [1]. Because of the relatively high doses involved, it is important that the benefit of a CT examination outweighs the risk the radiation exposure poses. This is ensured by optimising the procedure in order to keep the patient dose As Low As Reasonably Achievable (the ALARA principle).

2.1 The CT scanner

A CT scanner is based on the same principle as traditional radiography; radiation is attenuated differently in different body tissues, allowing different amounts of radiation to pass through. By detecting the radiation that passes through the patient (i.e. is not absorbed or scattered by the patient's body), an image of the inside of the body can be obtained. The principal difference between CT and traditional radiography is that a CT scanner obtains many consecutive images which, if stacked together, produce a three-dimensional image of the patient. From the outside, the CT scanner resembles a large ring, called the gantry. During a scan, the patient lies on a table which moves through the gantry while the X-ray tube and detector rotate around the patient. A schematic illustration of a CT scanner is shown in Figure 2.1.

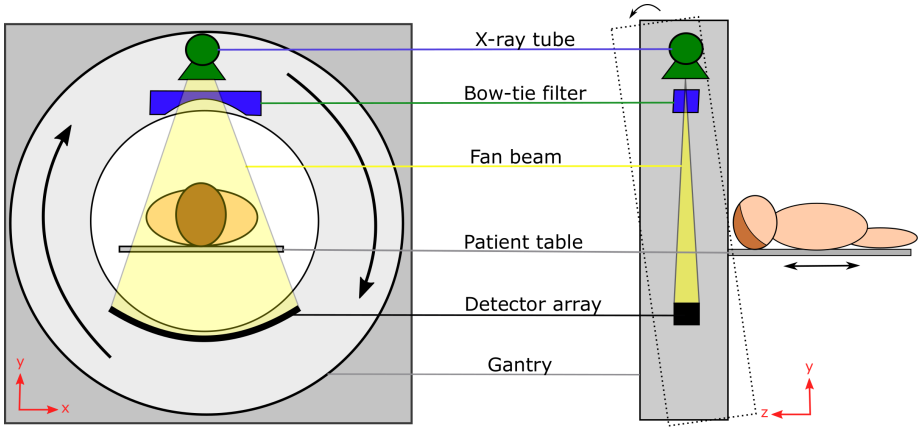

Figure 2.1: In a CT scanner, the patient lies on the movable patient table and is irradiated by a fan beam from an X-ray tube. The radiation passes through a bow-tie filter before radiating the patient and detected in the detector array. The tube, filter and detector array rotate around the patient. In some CT scanners the gantry can be tilted at an angle during the scan. Illustration inspired by [6].

The X-ray photons used to irradiate a patient are produced in an X-ray tube where a beam of high-energy electrons strikes the surface of a metal target. The source of these electrons is a heated, negatively charged cathode, often made of a tungsten wire [7]. The number of emitted electrons increases with the tube current. The electrons are accelerated towards the anode, which is often also made of tungsten, by the accelerating voltage (kV). When the electrons hit the target, a small part of their kinetic energy is converted into X-rays (approximately 1%), while the rest is lost as heat. The maximum X-ray energy occurs when all the kinetic energy of an electron is converted into a single photon, and this maximum photon energy is called the kilovolt peak (kVp). The majority of the X-rays produced result from so-called Bremsstrahlung, breaking radiation, which occurs when the electrons are decelerated near an atomic nucleus. This loss of kinetic energy is converted into X-rays, producing a continuous spectrum of X-ray energies lower than the kVp. In addition to this continuous spectrum there are peaks corresponding to the characteristic radiation from the anode material.

The fan-shaped photon beam in the CT scanner has a diameter of up to 70 cm [8] in the x-

and y-directions (depending on the tube angle) at the isocentre (the point at equal distances to all the positions of the radiation tube). This diameter is called the field of view (FOV), and is the maximum width that can be imaged at one time. The FOV is wide enough for most patients, allowing the entire patient volume to be included in the image. In the z-direction, the beam may be up to 16 cm wide [9], depending on the vendor and CT model.

On the opposite side of the X-ray tube in the gantry, there is a curved detector array which measures the intensity of the beam after it has passed through the patient. Detectors consist of a scintillator which converts the transmitted X-ray photons into visible light, and a photodiode which converts the visible light to an electrical current [10]. Then, the output current from each detector element is measured.

The intensity I of a photon beam passing through a body is attenuated according to Equation 2.1, where I_0 is the incoming intensity, μ is the attenuation coefficient of the body, and x is the distance the photon beam travels through the body.

$$I = I_0 \exp(-\mu x) \tag{2.1}$$

This means that the part of the fan beam which travels a short distance through the body is attenuated less than a part of the beam travelling a longer distance, provided μ is the same for the two distances. This means that more photons from the edges of the fan beam reach the detector, while fewer photons from the centre of the beam, which travel the longest distance through the patient, do the same. This difference may cause artifacts in the reconstructed image [7], and in order to avoid it, a bow-tie shaped filter is used. This filter reduces the intensity of the photon beam more at the edges than at the centre. A different filter is used to remove the lowest-energy photons, which are absorbed in the patient without contributing to the image formation. Removing them therefore decreases the patient dose without compromising the image quality. An example of the energy distribution of an unfiltered and filtered radiation beam is shown in Figure 2.2.

Some scanners allow the gantry to be tilted at an angle, as in Figure 2.1. This is mostly taken advantage of in head scans, where it is used to avoid irradiating the eye lenses, which are particularly radiosensitive [11], or dental fillings, which can cause artifacts (errors) in the image.

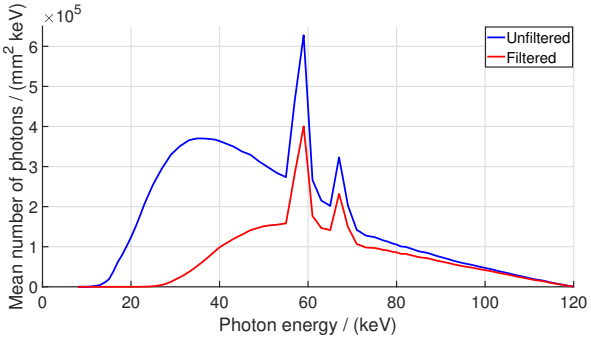

Figure 2.2: An X-ray spectrum with 120 kVp and tungsten as the anode material for an unfiltered beam (in blue) and a beam passing through a 0.3 mm copper filter (in red). The filter reduces the proportion of low-energy photons, and increases the average photon energy from 52 keV in the unfiltered beam to 64 keV in the filtered beam. The two distinct peaks are caused by photoelectric interactions, where characteristic X-rays are emitted as tungsten atoms relax to fill a vacancy in the K-shell, closest to the nucleus [12]. The spectra are generated using [13].

2.2 Obtaining CT images

When a patient is scanned, the patient table, with the patient on top, is moved in the z-direction. If the scanner rotates once and radiates one slice of the patient, then moves the patient one incremental step before scanning a new slice, the process is called sequential scanning. In practice, helical scanning is more common. Here, the patient table moves continuously in the z-direction while the patient is scanned by the rotating X-ray tube. Sequential and helical scanning are illustrated in Figure 2.3

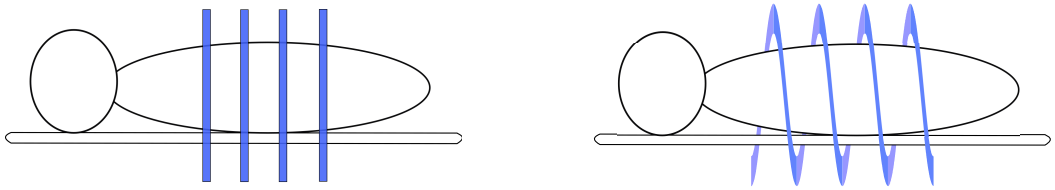

(a) Sequential

(b) Helical

Figure 2.3: The (a) sequential and (b) helical CT scanning modes. During sequential scanning, one slice is scanned at a time and the patient is moved between each slice scanning, while helical acquisition scans continuously while the patient is being moved. The distances between the imaged slices are exaggerated for illustrative purposes.

The photon beam from the radiation tube is attenuated as it passes through the patient. The value of μ depends on both the irradiated tissue and on the energy of the beam. When a given slice is scanned, projections are acquired from a large number of angles. For each projection, the detector array detects a large number of different intensities, which are interpreted as different attenuations in an attenuation profile. The attenuation profiles for all the angles are summarised in a sinogram,

where each horizontal line corresponds to a given angle, and each pixel value corresponds to an attenuation coefficient. The number of rows of the sinogram is equal to the number of angles each slice is imaged from. The information in the sinogram is used to reconstruct a two-dimensional image (a slice image) [7] by back-projecting (spreading evenly) each attenuation coefficient to create an image of the attenuation in each voxel (three-dimensional pixel) of the irradiated volume. The process, from detecting the radiation signal to producing a reconstructed image, is illustrated in Figure 2.4.

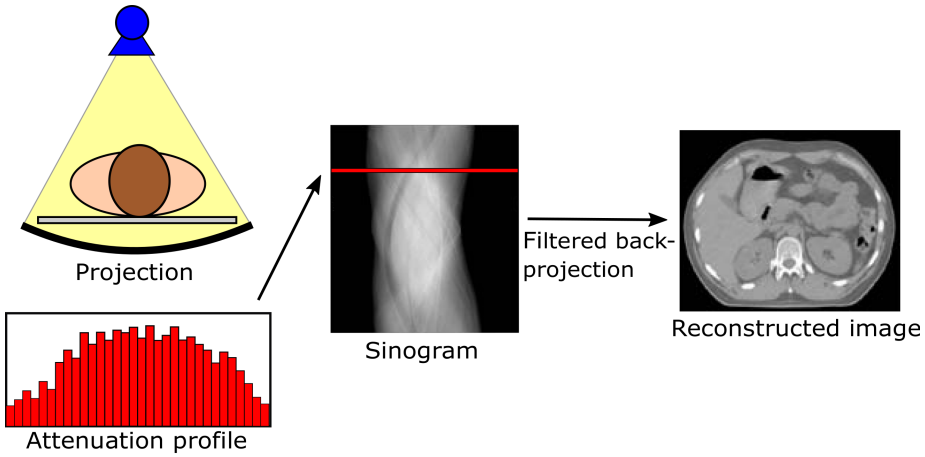

Figure 2.4: One projection of the patient is detected by the detector array at a time, producing the attenuation profile of the patient for one specific angle. A sinogram contains information about the attenuation profiles for projections from all the different angles. The information in the sinogram is used to reconstruct an image of the body through filtered back projection. The sinogram and reconstructed image are from [5].

A simple back-projection will result in a blurry image, which is compensated for by subjecting the signal to mathematical filtering. This is called a filtered back-projection (FBP), and its effect is illustrated in Figure 2.5.

The thickness of a typical voxel is in the order of millimetres [14]. The value of each voxel represents the average attenuation of the beam traversing the corresponding volume element.

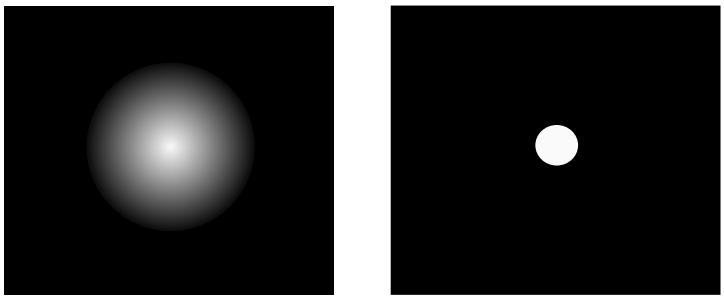

(a) Back-projection (b) Filtered back-projection

Figure 2.5: A white circle on a black background, illustrated for (a) back-projection and (b) filtered back-projection.

2.2.1 Pitch

The pitch p of a helical scan is defined as the ratio of the table feed TF (table movement per rotation) to the radiation beam width BW, as seen in Equation 2.2 [7]. The value of p determines the distance between each rotation of the tube relative to the patient, as illustrated in Figure 2.6.

$$p = \frac{TF}{BW} \tag{2.2}$$

If $p = 1$, the edges of the radiation beam line up (see Figure 2.6b). Decreasing or increasing the pitch results in the spiral pattern of the beam being respectively compressed (see Figure 2.6a) or extended (see Figure 2.6c).

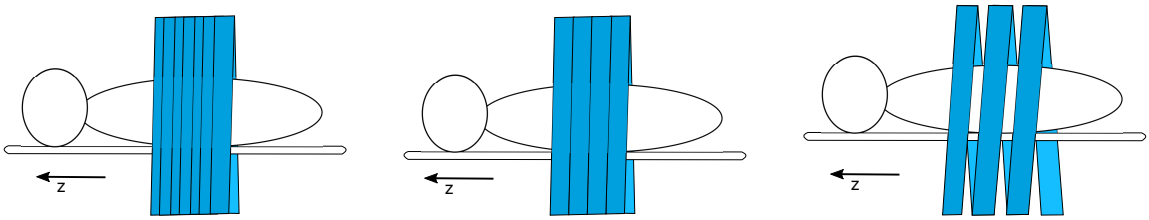

(a) $p < 1$ (b) $p = 1$ (c) $p > 1$

Figure 2.6: The patient is continuously moved in the z-direction. (a) When $p < 1$, there is an overlap in the radiation beam for each tube rotation. (b) When $p = 1$, the edges of the beam align without overlap. (c) When $p > 1$, the radiation beam forms a spiral with gaps between each rotation.

When $p = 1$, the patient is moved a distance in the z-direction equal to the BW during a 360°rotation, so that the centre of the patient (and the centre of the gantry) is irradiated once from each side for every rotation. As seen in Figure 2.7a, this causes large variations in the irradiation of different parts of the patient. Some areas are irradiated only once, some twice and some three times. When $p < 1$ the centre is irradiated more than once from each side for every rotation, because of the overlapping beam. This gives a more even dose distribution of the patient. With a

pitch of around 0.5, a large and uniform part of the field is irradiated three times, as illustrated in Figure 2.7b.

The advantage of a low pitch is that the image quality is higher due to a higher and more even dose per slice. However, a scan with low pitch takes longer to perform than one with a higher pitch. A higher pitch may therefore be used when the patient is unable to stay still in spite of the uneven radiation field and its consequences for image quality.

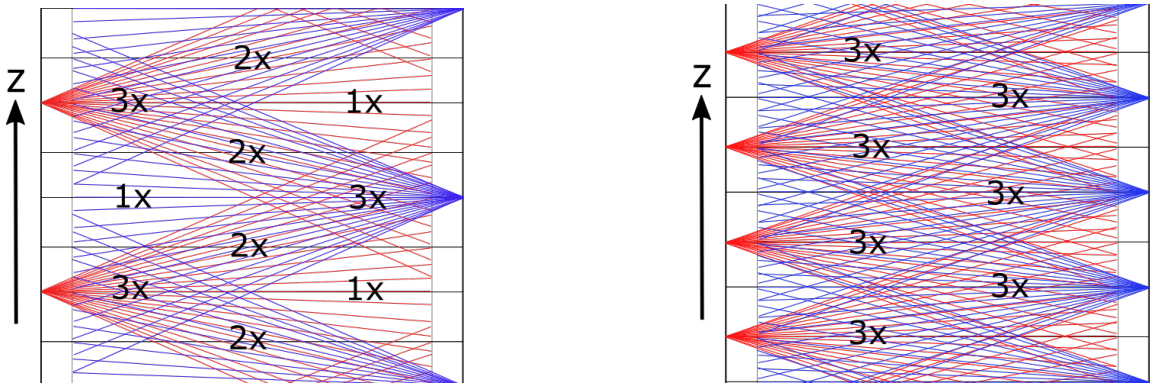

(a) $p = 1$ (b) $p = 0.5$

Figure 2.7: The radiation fields during a helical CT scan as seen from above. The number indicates the number of radiation beams passing through each area. (a) When $p = 1$ the amount of times an area is irradiated varies strongly with the position. (b) For $p = 0.5$ the distribution is more uniform, with most areas being irradiated three times.

2.2.2 Tube current modulation

Automatic tube current modulation (ATCM) was introduced for clinical use in 1994 [15] as a means of keeping the detector signal intensity constant throughout a scan, and therefore provide more consistent image quality. Today it is implemented in practically all CT scanners [16]. Since the radiation beam is attenuated differently in different parts of the body, ATCM increases the tube current when the beam is expected to be attenuated more, and decreases the tube current when less attenuation is expected. The expected attenuation over the range of the scan is estimated based on one or two scanned projection radiographs, where an image is acquired with a fixed tube angle while the patient table moves through the gantry [17]. The expected attenuation is then used to estimate the amount of current modulation needed.

ATCM is performed both in the scanning direction (along the z-axis), where is it called longitudinal modulation, and in the scanning (x-y) plane, where it is referred to as angular modulation [17]. The longitudinal modulation accounts for changes in attenuation along the length of the patient, for example by increasing the current when scanning the shoulders, and decreasing it when scanning the lungs. The angular modulation accounts for the body looking different from different angles. This is increasingly important where the cross-section of the body is elliptical, such as in the shoulders and pelvis. Here there is a large difference in how much the radiation beam is attenuated when passing through the shortest and longest body diameter. The angular modulation increases the current where the patient diameter is larger, and decreases it where the patient is

smaller. Longitudinal and angular modulation are illustrated in Figure 2.8.

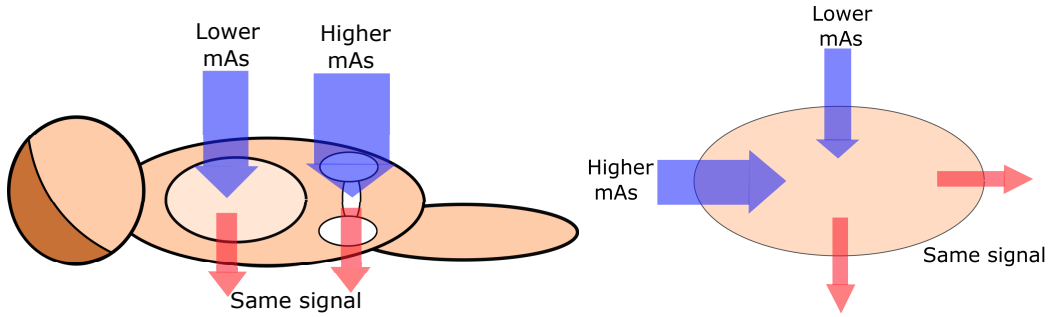

(a) Longitudinal modulation (b) Angular modulation

Figure 2.8: Blue represents entering photons, red represents exiting photons. The red arrows are the same size, giving the same signal to the detector. (a) A lower mAs is needed in the low-attenuating lung area than in the highly attenuating pelvis area. (b) A higher mAs is needed from the angles where the patient diameter is larger, and less where it is smaller.

Organ-based tube current modulation

In addition to modulating the current in order to keep the detector signal constant, the current can also be modulated to reduce the radiation exposure of specific radiosensitive organs. This is referred to as organ-based tube current modulation (OBTCM). Examples of sensitive organs which can receive lower organ doses with OBTCM techniques are the eye lenses and breasts. The fundamental idea behind OBTCM techniques is to reduce the tube current when the tube passes over the sensitive area. Depending on the philosophy of the vendor, the tube current may or may not be increased from the opposite direction in order to maintain the detector signal. Since the deposited dose of a ray of radiation is highest where the ray enters the body, the dose can be reduced on the anterior (the front of the body), and increased on the posterior (the back of the body) while still giving a lower organ dose to anterior organs, at the expense of higher dose to posterior organs. The angular width of the current reduction can be different for different body parts, e.g. smaller for head scans, as the eye lenses are centrally located, and larger for chest scans, as the breasts may cover a large area of a patient's chest. The details of the OBTCM techniques differ between manufacturers, and are further described in Chapter 3.

2.3 Image display

A widely used scale for interpreting CT scans is CT numbers, which are defined in Equation 2.3.

$$CT_0 = \frac{\mu_0 - \mu_{water}}{\mu_{water}} \cdot 1000 \tag{2.3}$$

Here, CT_0 is the CT number of a voxel, and μ_0 is the attenuation coefficient of the voxel. The CT numbers are expressed in the dimensionless units Hounsfield Units (HU) and represent the difference in attenuation relative to water. Since μ_0 depends on both the organ and the energy of

the incoming photons, substances other than water (which has a CT number of 0) have energy-dependent CT numbers [18], but less so than the attenuation coefficient. The CT number thus reduces the voxel value's dependence on the beam energy. The CT numbers in an image range from -1000 for air up to 3000 for dense bone. Some CT numbers for different tissues and organs are listed in Table 2.1.

Table 2.1: CT numbers of different tissues at 120 kVp. Data from [7, 19].

Tissue	CT number [HU]
Bone	1000 to 3000
Aorta	180 to 290
Liver	50 to 70
Muscle	30 to 50
Water	0
Fat	-70 to -100
Air	-1000

Each CT number is mapped to a shade of grey on a CT image; high CT numbers appear bright, while low CT numbers appear dark. Due to the large range of CT numbers in an image, bones may appear as featureless white areas, and the lungs equally featureless black areas [20]. When the image is displayed, the interesting range of CT numbers may be only a subset of the full range. The window width (WW) and window level (WL) can then be adjusted to change the appearance of the image, without changing the voxel values themselves. This allows fine structures in the image to be seen [20].

WL is the CT number of the "middle grey", the one in the middle between black and white. By lowering the WL the whole image is shifted to brighter tones, and by increasing WL the entire image becomes darker.

The WW is a measure on the "distance" from black to white, centred around the chosen WL. Every pixel value lower than WL $-\frac{\text{WW}}{2}$ is depicted as black, and pixel value higher than WL $+\frac{\text{WW}}{2}$ is depicted as white. Decreasing the WW is a way to better visualise small differences in voxel values in an image. In short, the brightness of the image is adjusted via the WL, and the contrast via the WW. An illustration of how WW and WL affect an image is shown in Figure 2.9.

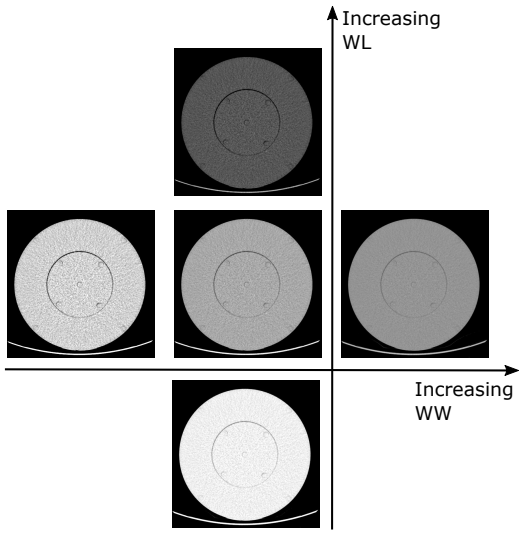

Figure 2.9: Changing WW and WL changes the appearance of an image without changing the pixel values themselves.

2.4 Dose

The absorbed dose D in a patient is a measure of how much radiation is absorbed per unit mass, and is defined as the ratio of absorbed energy to the tissue mass, as in Equation 2.4. The unit for absorbed dose is $\frac{\text{J}}{\text{kg}}$, or Gy.

$$D = \frac{\text{absorbed energy}}{\text{tissue mass}} \tag{2.4}$$

Different types of radiation (electromagnetic, α-, and β- radiation) may give the same absorbed dose, but different biological effects. A radiation weighing factor w_R is introduced to reflect this difference. The so-called equivalent dose accounts for the difference in biological effect. The equivalent dose H_T to an organ or tissue radiated by radiation type R is defined according to Equation 2.5, where D_T is the absorbed dose in organ T, from the radiation type R. For X-rays, $w_R = 1$. Equivalent dose, or organ dose, is measured units of Sievert (Sv = $\frac{J}{kg}$).

$$H_T = w_R \cdot D_{T,R} \tag{2.5}$$

Different organs and tissues have different sensitivities to radiation, and a tissue weighing factor w_T is therefore introduced. It represents the fraction of the total stochastic radiation risk to each organ, for all the different organs and tissues. Multiplying the equivalent dose by the tissue weighting factor, and summing over all tissues, gives the effective patient dose D_{eff} as in Equation 2.6. The unit for D_{eff} is Sv, and the values of w_T for the different organs can be seen in Table 2.2.

$$D_{eff} = \sum_T H_T \cdot w_T \tag{2.6}$$

Table 2.2: The tissue weighing factor w_T for different organs. The sum of w_T for all organs is 1.

Organ	w_T [1]
Breasts	0.12
Lung	0.12
Colon	0.12
Red bone marrow	0.12
Stomach	0.12
Gonads	0.08
Bladder	0.04
Liver	0.04
Thyroid	0.04
Oesophagus	0.04
Brain	0.01
Bone surface	0.01
Salivary glands	0.01
Skin	0.01
Remainder of body	0.12

CT scans are associated with a higher radiation dose than other imaging modalities, and therefore involve a greater risk of the patient developing radiation-induced cancer according to the linear no-threshold model. However, the knowledge gained from a CT scan is often crucial in saving the patient's life. It is important that the benefit of the examination outweighs the risk involved, and that the procedure is optimised according to the ALARA principle.

2.4.1 CT doses

In traditional projection radiography, the patient is irradiated from only one or a few angles. Due to the attenuation of the radiation beam in the body, there are more photons entering the body than exiting the body. This means that the beam deposits a higher dose closer to the radiation tube, and the deposited dose decreases toward the point the beam exits the body, as shown in Figure 2.10a.

The situation is different for CT scans, where the patient is irradiated from all angles as the radiation tube rotates around her. If the imaged object is spherical and homogeneous, the dose distribution in the object in a CT scan will be spherically symmetric, with the highest dose at the periphery and lowest in the centre. This is illustrated in Figure 2.10b. The dose in the centre is approximately half of the surface dose. Since the dose distribution in CT is so different from traditional radiography, dose quantities used in traditional radiography are not applicable to CT [21].

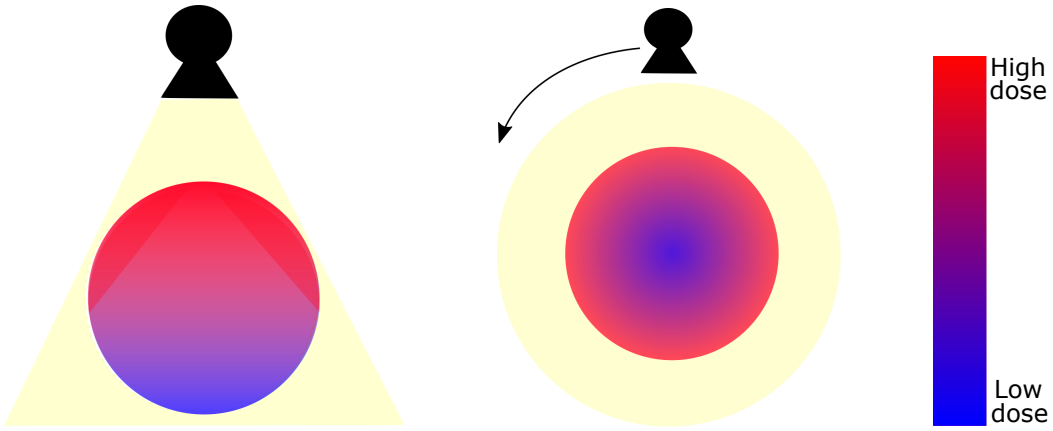

(a) (b)

Figure 2.10: (a) In traditional X-ray radiography, the dose is highest (indicated by red colour) where the beam enters the body, and lower where it exits the body (indicated by blue colour). (b) In CT scans, the dose distribution in a homogeneous, spherical body is spherically symmetric because the body is irradiated from all angles by the rotating X-ray tube.

The radiation output from the X-ray tube can be described by the tube current-time product (mAs), which is the product of the tube current and the tube rotation time. The mAs reflects the total number of X-ray photons the X-ray tube produces. The mAs is proportional to the radiation dose the patient receives, and can therefore be used to indicate the delivered dose of a scan. It is, however, not appropriate to compare doses for different patients and different CT scanners in terms of the mAs, as the proportionality constants will be different.

The dose received by a patient during a CT scan is often evaluated by two dose descriptors: the computed tomography dose index (CTDI) and the dose-length product (DLP). CTDI is a measure of the local dose, while DLP represents the dose associated with the full CT scan. Both these dose descriptors represent an estimated dose to a standard phantom, and are estimated prior to each patient scan based on the selected exposure parameters. The estimated values are provided to the operator, who has the option of adjusting the exposure parameters in order to optimise the procedure.

2.4.2 Computed tomography dose index

The CTDI describes the dose delivered by a single rotation of the X-ray source [21], and has units milligray (mGy). The majority of the dose is deposited inside the radiation beam, but due to scattering some dose will also be delivered outside of the beam. The CTDI sums up the dose contribution along the z-axis, accounting for dose delivered both inside and outside of the beam width. It represents what the total delivered dose would be if all the dose was delivered inside the beam width. For a scan with multiple rotations, the CTDI is equal to the average level of the total dose profile, provided that the pitch is equal to 1 [21]. CTDI is illustrated in Figure 2.11. Mathematically, CTDI is defined according to Equation 2.7, where $D(z)$ is the dose value at point z, and BW is the radiation beam width.

$$\text{CTDI} = \frac{1}{BW}\int_{-\infty}^{\infty} D(z)dz \tag{2.7}$$

In practice, the dose is often summed from -50 mm to $+50$ mm relative to the centre of the beam, instead of summing to infinity, and the resulting quantity is called the CTDI_{100}.

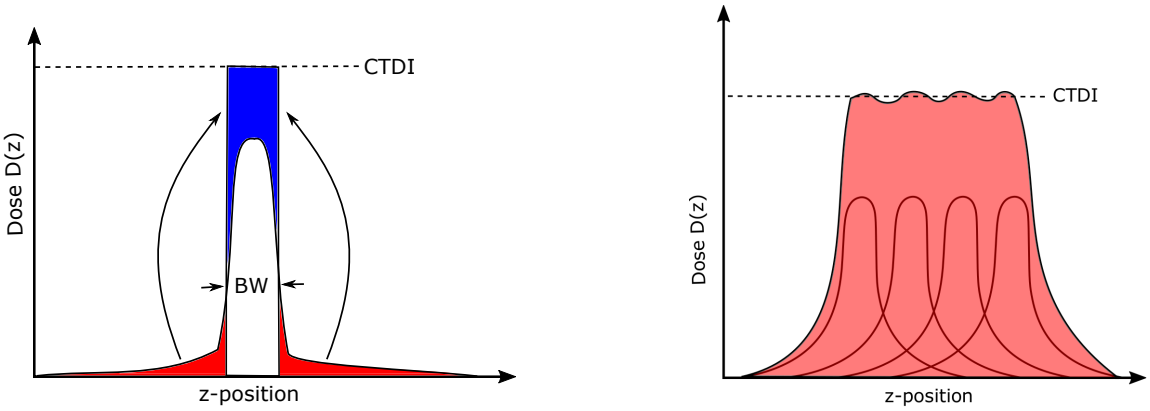

(a) (b)

Figure 2.11: (a) The CTDI represents the total dose given by one tube rotation. The dose deposited outside of the beam width (blue) is "shifted" inside the beam width in order to make a rectangle of width BW and height CTDI. (b) The total dose profile of a scan with 4 rotations. When the pitch is equal to 1, the CTDI is equal to the average level of the total dose profile.

Because the CTDI is measured at a point in the x-y plane, the measured value depends on the position where it is measured. The CTDI generally refers to measurements in standard dosimetry phantoms with patient-like diameters [21]. In such CTDI phantoms, the CTDI_{100} can be measured in four positions along the periphery and one in the centre of the phantom by using an ionisation chamber. A cross section of such a CTDI phantom is illustrated in Figure 2.12.

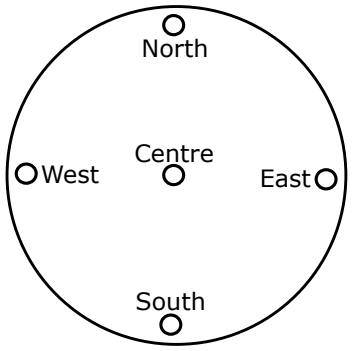

Figure 2.12: A CTDI phantom, where $\text{CTDI}_{\text{centre}}$ is measured in the centre hole, and $\text{CTDI}_{\text{periphery}}$ is the average of the measured values in the North, East, South and West positions. The standard diameters of this kind of phantom are 160 and 320 mm in order to represent the size of a patient's head and trunk, respectively.

In order to account for the dose varying across the cross-section, the weighted CTDI, CTDI_w is defined according to Equation 2.8.

$$\text{CTDI}_w = \frac{1}{3}\text{CTDI}_{100,\text{ centre}} + \frac{2}{3}\text{CTDI}_{100,\text{ periphery}} \tag{2.8}$$

Here $\text{CTDI}_{100,\text{ centre}}$ is the measured CTDI_{100} in the centre of the phantom, and $\text{CTDI}_{100,\text{ periphery}}$ is the average of the four measured CTDI_{100} along the periphery.

The dose to a given volume depends on the pitch of the scan, i.e. from how many tube rotations the volume is irradiated. The volume CTDI, CTDI_{vol}, is the pitch-corrected CTDI_w, and is defined according to Equation 2.9.

$$\text{CTDI}_{vol} = \frac{\text{CTDI}_w}{p} \tag{2.9}$$

2.4.3 Dose-length product

The DLP is used to compare the delivered dose in scans of different lengths. It is defined as the product of the radiation intensity (represented by CTDI_{vol}) and the scan length L [21], as shown in Equation 2.10.

$$\text{DLP} = \text{CTDI}_{vol} \cdot L \tag{2.10}$$

The DLP has units mGy·cm, and is a measure of the total dose delivered during a CT scan. It does not, however, reflect the dose absorbed by the patient during a scan. A DLP of 500 mGy·cm delivered to a small patient gives a higher patient dose than 500 mGy·cm delivered to a large patient. DLP is therefore a useful quantity when comparing the doses delivered by different scanners, but not for comparing doses to different patients.

2.4.4 Radiation-induced effects

The biologic effects caused by X-rays, and ionising radiation in general, are a result of damage inflicted on the DNA of the cells in the body. The DNA can be damaged directly through ionisation by an incoming photon, or by fast-moving electrons from other ionised molecules. Alternatively, the damage can be indirect, caused by water being ionised and forming free radicals, which react with and break chemical bonds in nearby DNA molecules [20].

The cells are better able to repair many small DNA damages over a long period of time than a few large damages in a short time span. Therefore, a single high dose has a greater potential for damage than frequent exposure to low doses. If the damage from an exposure is not repaired, the affected cells may die or lose their ability to proliferate. This is the cause of acute, or deterministic, radiation effects. A deterministic effect will occur when a certain dose threshold is exceeded, and the severity of the effect increases with a further increase of dose [12]. If a repair is unsuccessful, the cell may stay alive and proliferate in a mutated form. Such mutation can cause carcinogenic effects and may result in cancer. Carcinogenesis is a stochastic effect, meaning that the probability of developing cancer increases with dose, probably with no threshold, but the severity of the cancer is not related to the dose [12].

Data from atomic bomb survivors indicate that there is a linear relationship between dose and cancer induction in a lin-log diagram for the high doses of more than 100 mSv [22]. For lower doses, the data indicates that the increase in radiation-induced cancer is too small to be distinguished from other cases of cancer [22]. Due to the lack of data for doses below 100 mSv, a hypothetical model must be employed to extrapolate the results found for high doses to the lower doses (a few mSv) associated with medical imaging. Various attempts of doing so are illustrated as dashed lines in Figure 2.13. The most commonly used model, which also is the simplest, is the linear no-threshold (LNT) model shown as a dashed black line. This model extrapolates the linearity at high doses to the low dose domain, giving a completely linear model in a lin-log diagram of radiation-induced cancer risk as a function of dose. The LNT model says that any level of radiation increases the risk of developing cancer, even the relatively low doses associated with CT scans. Doses from typical radiologic examinations lie well below 100 mSv, as shown in Table 2.3.

Table 2.3: Typical effective doses for some common radiologic procedures performed in Norway in 2008. Data from [1].

Procedure	Effective dose [mSv]
Chest radiograph	0.07
Mammography	0.15
Abdomen radiograph	1.2
CT head	1.5
CT thorax	4.7
CT abdomen	10

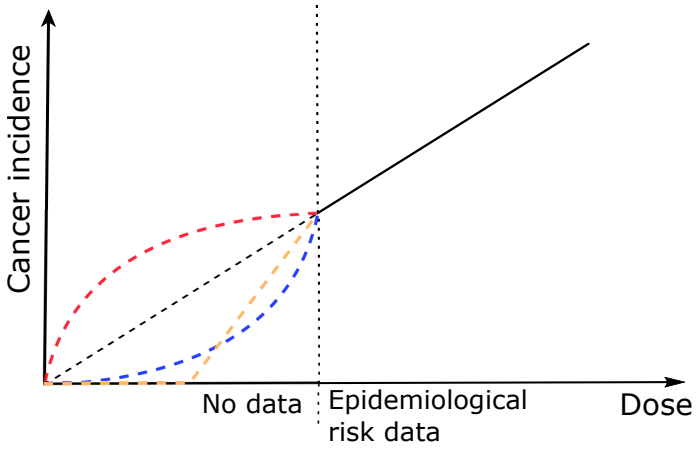

Figure 2.13: Epidemiological risk data from atomic bomb survivors indicate that for high doses above 100 mSv, the dose- cancer incidence relationship is linear in a lin-log plot (solid black line). At low doses there are several models, due to a lack of data, where the linear no-threshold model (solid black and dashed black line) is the most common. This model extrapolates the linear dose-risk relationship to low doses, indicating that any amount of radiation increases the risk of developing cancer. Other models, here shown in dashed red, blue and orange, behave differently at doses below 100 mSv.

2.4.5 Selected radiosensitive organs: breasts and eye lenses

The breasts are among the organs with the highest tissue weighing factor, after it was increased in 2007 by the International Commission on Radiological Protection (ICRP) [23]. Although breasts are not normally an organ of interest in chest CT examinations, they are included in the radiation field and receive a considerable amount of dose [24].

In recent years there has been an increasing awareness of the radiosensitivity of the eyes. Up until 2017, the laws in Norway and the EU prohibited that the annual equivalent dose to the eye lenses of radiation workers exceeded 150 mSv. This was based on research from the 1950s. In the last decade, there has been research suggesting that this limit is too high, and on 1st of January 2017 the regulations in Norway ("Strålevernforskriften") reduced the limit to 20 mSv of annual equivalent dose to the eye lenses, in accordance with ICRP's recommendations [25].

2.5 Image quality

There are several ways to evaluate image quality, but what determines if an image is good or not depends on both the situation and the subjective opinion of the one evaluating the quality. There is no universal measure of image quality, as different tasks require different images [26]. In CT imaging there are several parameters that are used to describe image quality, including noise, signal-to-noise ratio, contrast-to-noise ratio, CT number accuracy and spatial resolution [27]. However, current literature that focuses on the relationship between dose and image quality generally explores only one or a few such parameters [27]. In this thesis the image noise is used as the parameter describing image quality.

2.5.1 Image noise

A CT image of a uniform and homogeneous area will not have a constant voxel value, it will fluctuate around some mean value. These unwanted fluctuations in the voxel values are noise. Since the CT numbers of voxels in images are used to differentiate between different soft tissues within the human body, noise degrades the diagnostic quality of CT images [28].

Because CT noise appears as a fluctuation in CT numbers, measurements of image noise are based on these fluctuations. One way to do this is to measure the standard deviation of CT numbers within a uniform region of interest (ROI) in the image, where the CT numbers should have the same value. The amount of noise in the ROI is said to be this standard deviation of CT numbers, with higher standard deviations reflecting higher levels of image noise

A major contribution to the noise in CT images is statistical noise, stemming from fluctuations in the finite number of X-ray photons that are detected. Statistical noise is also called quantum noise, and as more X-ray quanta are detected, the relative fluctuations become smaller.

The only way to reduce the statistical noise is to increase the number of X-ray photons, normally achieved through increasing the X-ray tube current and thereby increase the patient dose [28]. The statistical noise σ_s decreases as the inverse of the square root of the dose, as in Equation 2.11.

$$\sigma_s \propto \frac{1}{\sqrt{D}} \tag{2.11}$$

This relationship assumes radiation symmetry, i.e. that the tube current is constant throughout the scan. A reduction of noise is therefore a trade-off for increased image quality at the expense of increased patient dose. Figure 2.14 shows how the noise is reduced as the dose is increased.

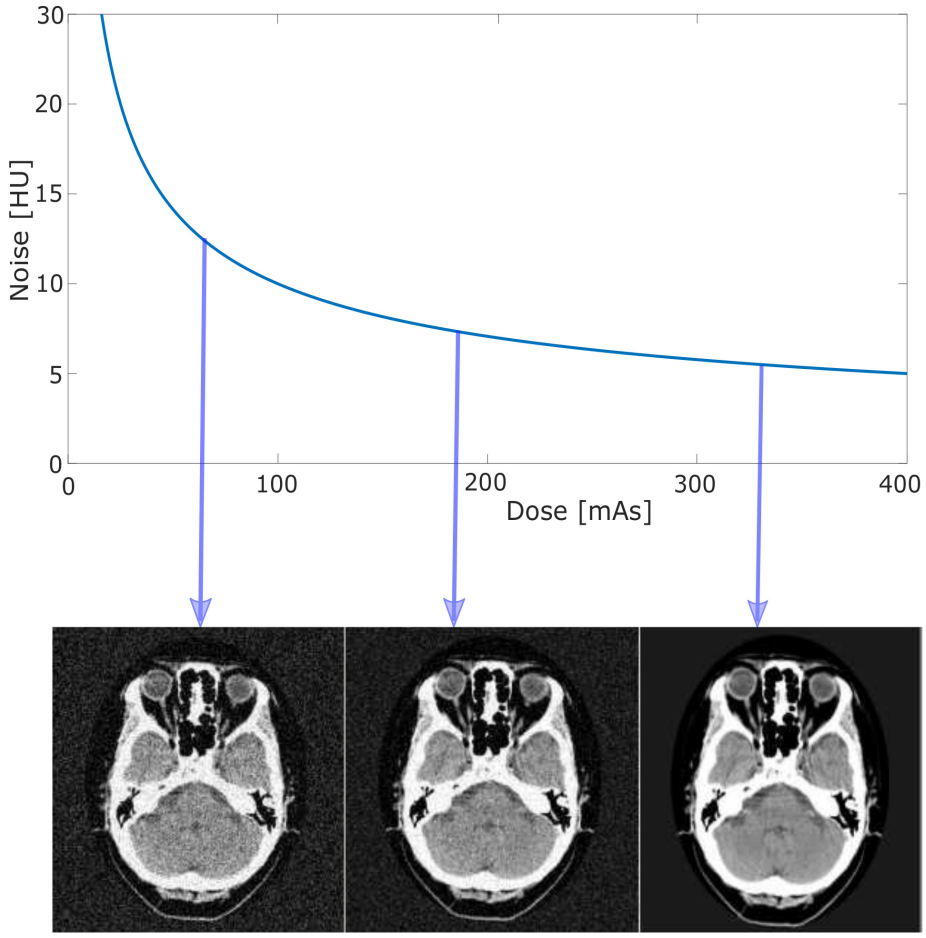

Figure 2.14: Noise in a CT image decreases as the inverse of the square root of the dose, with lower noise giving clearer images. CT images based on [29].

Chapter 3

Materials and Methods

In this thesis, the CT scanners Siemens Somatom Definition As+ (Siemens Healthcare, Forchheim, Germany) and GE Revolution (GE Healthcare, Waukesha, Wisconsin, USA), were used to investigate OBTCM techniques for dose reduction to the eye and breast from the two respective vendors. The GE scanner is located at Haraldsplass Diakonale sykehus (HDS), and the Siemens scanner at Haukeland University Hospital (HUH). Two phantoms, one ATCM phantom and one CTDI phantom, were scanned without and with OBTCM. The dose reduction and its impact on the noise in the resulting images were analysed, and the vendors' different approaches were evaluated and compared.

3.1 The CTDI phantom

The CTDI phantom (RTI, Mölndal, Sweden) is a cylindrical phantom made of polymethyl methacrylate (PMMA), of length 150 mm with holes of diameter 13 mm where a detector can be inserted. The CTDI phantom consists of a cylinder with diameter 160 mm, referred to as the "head phantom", and a larger annulus of diameter 320 mm. When the head is inserted into the annulus, they make up the "body phantom" together. The head- and body CTDI phantoms are shown in Figure 3.1. The holes are placed in the periphery, 10 mm from the edge of both the head and body, and the head has an additional hole in the centre. A detector can be inserted into one of the holes during the CT scan in order to measure the imparted dose in that position. Plugs can be inserted into the holes that are not in use.

(a) Head (b) Body

Figure 3.1: The CTDI (a) head and (b) body configuration. In (a) the plug at the North position is removed, so that a detector can be inserted.

3.2 The ATCM phantom

The CCT228 ATCM phantom (The Phantom Laboratory, Greenwich, New York, USA) is designed as an aid for ATCM testing and optimisation [30]. The ATCM phantom, shown in Figure 3.2, is made of uniform PMMA and has no internal structures, which makes it well-suited for investigating image noise.

The phantom consists of three elliptical sections with different dimensions; a small, a large and a medium section. All the sections have a ratio of 3:2 between the x- and y-directions, or the width and height. The edges between the sections are smoothed to eliminate hard edge transition artifacts [30]. The dimensions of each section are shown in Table 3.1. The length of the phantom is 630 mm in the z-direction.

The different sections make it possible to examine how the images are affected by the size of the phantom. For each of the two scanners, the phantom was scanned once with a standard scan and once with the OBTCM technique, and the images of each section were used to examine the noise in that section. In addition, the phantom was scanned with an overall reduction of mAs of 40%

Figure 3.2: The ATCM phantom is elliptical with a small, large and medium section.

relative to a standard scan.

Table 3.1: The dimensions of each section of the ATCM phantom [30]. D_x and D_y are the diameters in the x- and y-direction, respectively.

	D_x [mm]	D_y [mm]
Small end section	250	167
Large middle section	350	233
Medium end section	300	200

3.3 Organ-based tube current modulation

This thesis investigates and compares Siemens' and GE's approaches to using OBTCM to reduce the dose to the eye lenses and breasts. The vendors have chosen two different approaches to the problem; Siemens aims to keep image quality constant, while GE allows more noise and gives an overall dose reduction to the patient. In order to reduce the dose to these sensitive organs, both vendors have developed techniques which reduce the tube current on the anterior of the patient, where both the eye lenses and breasts are located. The difference lies in what happens to the tube current during the remainder of the tube rotation; Siemens increases the current, while GE keeps it at the original level.

3.3.1 Siemens: X-CARE

Siemens offers the OBTCM technique X-CARE on their CT scanners. When X-CARE is used, the radiation intensity is reduced when the patient is irradiated from the anterior, and increased when the patient is irradiated from the posterior. X-CARE reduces the current in the upper 120° of the rotation, while increasing the current in the lower 240° for both breast and head protocols as illustrated in Figure 3.3.

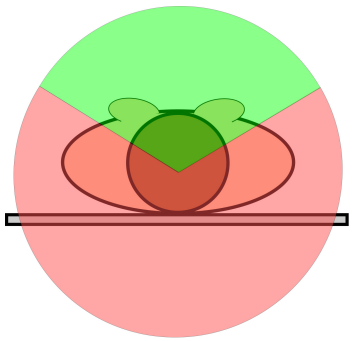

Figure 3.3: X-CARE reduces the tube current in the top 120°(green area) of the scan in order to shield the eye lenses and breasts. The tube current is increased in the remaining part of the rotation (red area) in order to maintain the image quality.

This is done in a manner that keeps the average $CTDI_{vol}$ constant and therefore also keeps the detector signal constant, and thus maintains the image quality. This is possible because X-CARE operates with a pitch of 0.55 and therefore have two complementary projections from every angle throughout the rotation. Since the attenuation coefficients of two complementary projections are the same, the total detector signal along the paths will not be affected by distributing the patient dose differently along the two projections. By reducing the current from one direction and increasing the current from the opposite direction, the surface area of the patient that is irradiated with a lower current receives a lower skin dose. Eye lenses and breasts are sensitive organs that are located close to the surface and therefore receive a lower dose when this technique is used. An illustration of why it is possible to reduce the dose absorbed in a region without increasing the noise of the region is shown in Figure 3.4. The indicated numbers are fictitious, and assume that 90% of the radiation is absorbed in the patient,in order to illustrate that the detector signal is equal in the two cases. A rough estimate gives 90% attenuation of a beam with 120 kV after it has passed through 11 cm of soft tissue [31].

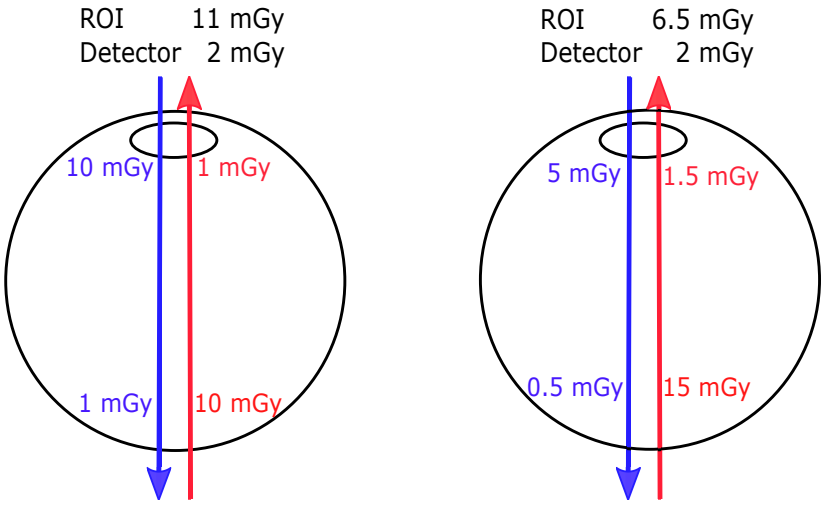

(a) Standard (b) X-CARE

Figure 3.4: It is possible to reduce the dose to a ROI (small black ellipse) without a corresponding increase in noise in the same region. This is because the patient dose and detector signal are different concepts, and the patient dose may be redistributed without affecting the detector signal. (a) The anterior (blue) and posterior (red) projections indicate incoming and outgoing radiation. 1 mGy contributes to the detector signal from each direction, giving a total of 2 mGy. The ROI receives 10 mGy from the anterior projection and 1 mGy from the posterior projection, a total of 11 mGy. (b) The anterior projection delivers a dose of 5 mGy to the ROI, while the posterior projection delivers a dose of 1.5 mGy to the ROI. The total detector signal is the same as for the standard scan (2 mGy), but the dose to the ROI is lower (6.5 mGy compared to 11 mGy for the standard scan).

3.3.2 GE: ODM

GE offers the OBTCM technique Organ Dose Modulation (ODM) on their CT scanners. ODM distinguishes between head and chest protocols; for head protocols the tube current is reduced in the upper 90° of the rotation (see Figure 3.5a), whereas the chest protocol reduces the tube current in the upper 150° or 180° part of the rotation. The sector of dose reduction for the chest protocols varies between scanner models. The GE Revolution scanner, which was used in this thesis, has a sector of current reduction of 150°, as shown in Figure 3.5b. As opposed to X-CARE, ODM does not boost the tube current in the lower part of the rotation. This gives a reduction in the total patient dose at the expense of the image quality.

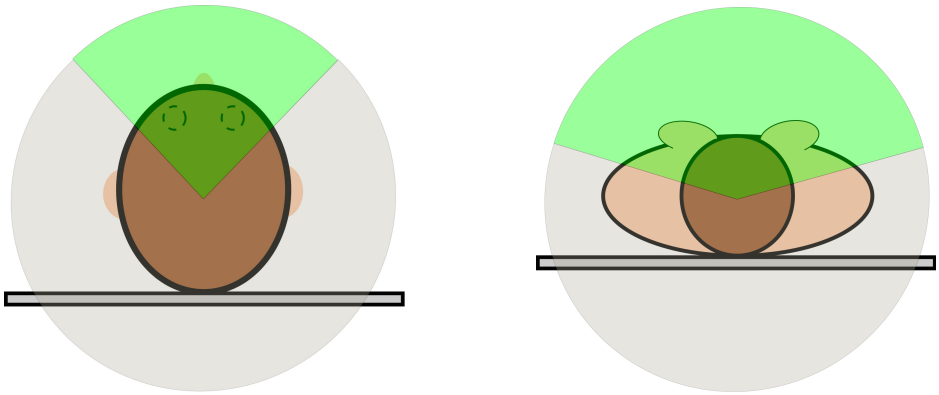

(a) ODM head protocol (b) ODM chest protocol

Figure 3.5: (a) ODM reduces the current in the upper 90° of the rotation (green) for the head protocol, without increasing the current from below. The positions of the eyes are indicated by dashed circles. (b) In the chest protocol the current is decreased in the upper 150° of the rotation.

3.4 An alternative to OBTCM: reducing the tube current

If OBTCM techniques are not available, the same dose reduction to the eye lenses and breasts can be achieved by reducing the total delivered dose, at the expense of increased image noise. Since both Siemens and GE claim a dose reduction to eye lenses and breasts of about 40% when OBTCM techniques are used, the ATCM phantom was scanned with a standard chest protocol, but with a global reduction of mAs of 40% for both the Siemens and GE scanner. The image noise in these "low mAs" scans was then compared to the standard scans.

3.5 Protocol specifications

The settings used during the CT scans in this thesis are shown in Table 3.2 for the ATCM phantom and in Table 3.3 for the CTDI phantom. For all scans, the ATCM and CTDI body phantoms were scanned with chest protocols, and the CTDI head phantom was scanned with head protocols. Both phantoms were positioned in the centre of the gantry during the scans.

Table 3.2: The protocols used during the CT scans of the ATCM phantom in this thesis. Coll refers to collimation, Filter is a reconstruction filter, ST is the slice thickness of the reconstructed images, FoV is the field of view, NI is noise index, and Rot. time means rotation time. For the Siemens scanner, kV and Quality Reference (QR) mAs are given, for GE kVp and mA are given. QR mAs is a parameter defined by Siemens, representing the image quality that would have been achieved if a fixed tube current examination had been performed at that specific mAs for an average sized patient [32].

Vendor	Phantom	Technique	kVp	QR mAs/mA	Coll.[mm]	NI	Rot.time[s]	Pitch	ST[mm]	Filter	FoV[mm]	$CTDI_{vol}$[mGy]
Siemens	ATCM	Standard	100	110	128·0.6	-	0.3	0.55	3	B31f	400	4.01
Siemens	ATCM	X-CARE	100	110	128·0.6	-	0.3	0.55	3	B31f	400	4.14
Siemens	ATCM	Low mAs	100	110	128·0.6	-	0.3	0.55	3	B31f	400	2.43
GE	ATCM	Standard	120	40-720	64·0.625	26.5	0.35	0.516	3	Standard	450	7.7
GE	ATCM	ODM	120	40-720	64·0.625	26.5	0.35	0.516	3	Standard	450	6.1
GE	ATCM	Low mAs	120	40-720	64·0.625	33.5	0.35	0.516	3	Standard	450	4.6

Table 3.3: The protocols used during the CT scans of the CTDI phantoms in this thesis. Coll refers to collimation, Filter is a reconstruction filter, ST is the slice thickness of the reconstructed images, FoV is the field of view, NI is noise index, and Rot. time means rotation time. For the Siemens scanner, Quality Reference (QR) mAs is given, for GE mA is given.

Vendor	Phantom	Technique	kVp	QR mAs/mA	Coll.[mm]	NI	Rot.time[s]	Pitch	ST[mm]	Filter	FoV[mm]	$CTDI_{vol}$[mGy]
Siemens	CTDI body	Standard	100	110	128·0.6	-	0.3	0.55	3	B31f	350	7.51
Siemens	CTDI body	X-CARE	100	110	128·0.6	-	0.3	0.55	3	B31f	350	7.50
Siemens	CTDI head	Standard	120	350	32·1.2	-	0.3	0.55	3	H31s	200	49.5
Siemens	CTDI head	X-CARE	120	350	32·1.2	-	0.3	0.55	3	H31s	200	49.7
GE	CTDI body	Standard	100	240	64·0.625	25	0.35	0.516	3	Standard	360	7.1
GE	CTDI body	ODM	100	190	64·0.625	25	0.35	0.516	3	Standard	360	5.7
GE	CTDI head	Standard	120	370	64·0.625	3.6	0.35	0.516	3	Standard	230	49.7
GE	CTDI head	ODM	120	345	64·0.625	3.6	0.35	0.516	3	Standard	230	44.8

3.6 Dose measurements

For each of the two CT scanners, the CTDI head and body phantom were scanned three times with a detector placed in one of the holes, both with and without the OBTCM techniques. This was repeated for all the holes. The detector measured the accumulated DLP in each position. The detector is shown in the centre position of the CTDI body phantom in Figure 3.6.

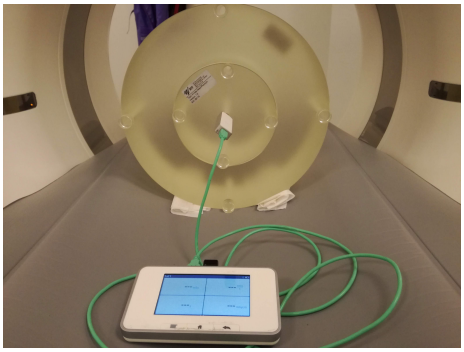

Figure 3.6: The DLP in the centre of the phantom was measured by scanning a short section of the phantom with a detector inserted into the centre hole, and repeated three times. The DLP in the different positions were measured in the same way, and plugs were inserted into the holes not in use.

During these scans, the phantom was positioned so that one of the periphery holes was located in the North (N) position. After performing scans with the detector in the centre and in all the peripheral positions, the phantom was then rotated 45°and the measurements along the periphery were repeated. This resulted in the dose being measured in the North, North East, East, South East, South, South West, West, North West and centre positions. These positions are illustrated in Figure 3.7. The doses in the different areas with OBTCM were calculated relative to the doses of the standard scan. For each scanner, nine measuring points were scanned three times, resulting in 27 scans for each setup without and with OBTCM.

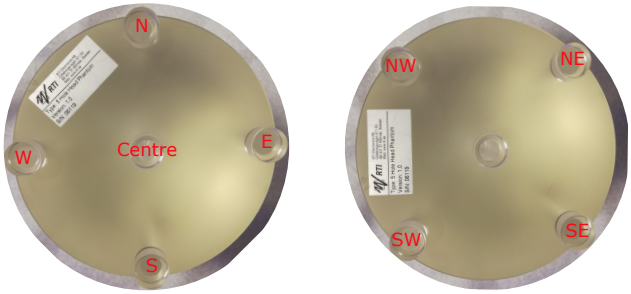

(a) (b)

Figure 3.7: The DLP was measured in each of the (a) centre, North, East, South, West, and (b) North East, South East, South West and North West positions of both the head and body phantom.

Normally, the CTDI phantom would be used to measure $CTDI_{100}$, but because areas greater than the slice thickness were scanned, the $CTDI_{100}$ has to be calculated from the measured DLP. In addition, $CTDI_{100}$ should be based on sequential scans, but the OBTCM techniques can only be used during helical scans. As it is the *relative* doses that are interesting when a scan without and with OBTCM are compared, the dose measurements in this thesis are based on the directly measured DLP.

3.7 Noise measurements

Statistical analysis on image noise was performed with a two-sample t-test for equal means without assuming equal variances (ttest2, Statistical toolbox, MATLAB, The MathWorks, Inc.).

3.7.1 Noise in different ROIs in the CTDI phantom

One way to describe the distribution of noise in the images of the CTDI phantom is to choose different ROIs corresponding to the positions where the dose is measured. In order to measure the noise in homogeneous areas, the measurements were performed at the North, East, South, and West positions with the holes between these positions, as shown in Figure 3.8a for the head phantom. This was done due to the holes producing a large amount of image noise. The circular ROIs along the periphery were chosen to have a radius of 10 mm. Due to the hole in the centre of the phantom, the noise at the centre was measured by having four smaller ROIs of radius 5 mm (and a total area equal to a 10 mm radius ROI) were placed around the centre and the average of these used as the noise in the centre. These small ROIs are shown in Figure 3.8b for the head phantom. These measurements were performed on both the head and body CTDI phantoms.

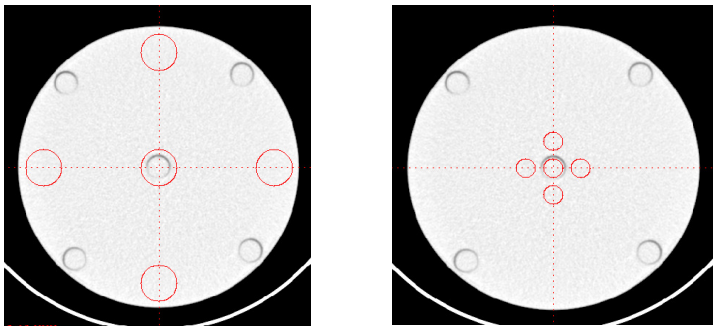

(a) (b)

Figure 3.8: The circular ROIs used to calculate the noise in the obtained images of the CTDI phantom, here shown for the head (16 cm) phantom. (a) Four ROIs of radius 10 mm along the periphery of the phantom give the noise of the image series in the North, East, South and West positions. The centre ROI was not used because of noise from the hole. (b) The four ROIs have a total area equal to one of the ROIs on the periphery, and the average of these four give the noise in the centre. The ROI at the centre was not used.

3.7.2 Noise in the ATCM phantom

Since the ATCM phantom is made of a uniform material, but with variations of diameter along the z-axis, this can be used to investigate whether X-CARE maintains the noise level of the standard scan for different patient sizes. It can also be used to examine whether the amount of noise in ODM scans is affected by the patient size. This was investigated by calculating the noise within a ROI for each image throughout the series of images of each section. This gave the amount of noise within each section of the ATCM phantom, and how the noise varied between the sections. The program ImageQC [33] was used to calculate the noise in the phantom. A circular ROI was placed in the centre of the image, and the size was adjusted so that the radius of the ROI was equal to half of the smallest radii, for each section of the ATCM phantom. The ROI in the small section had a radius of 41.8 mm, the large section 58.3 mm and the medium section 50 mm. These ROIs were applied to each image in a series. The size and position of the ROIs are shown in Figure 3.9.

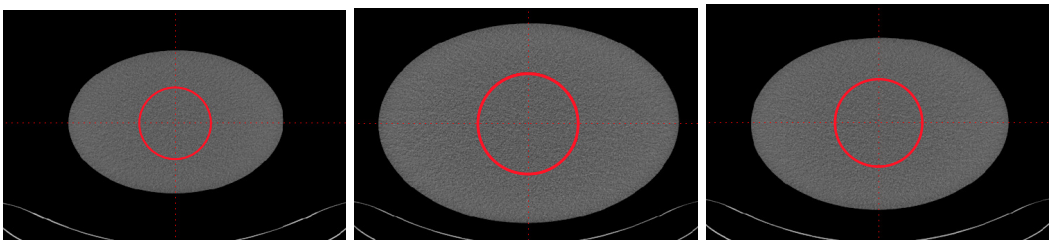

(a) Small section (b) Large section (c) Medium section

Figure 3.9: The circular ROI used to calculate the noise in the obtained images of the ATCM phantom. The ROI has a radius equal to half of the smallest radius of each section, i.e. (a) a radius of 41.8 mm for the small section, (b) a radius of 58.3 mm for the large section, and (c) a radius of 50 mm for the medium section.

3.7.3 Noise maps

Since noise is a measure of the standard deviation within a ROI, it means that the area where the noise is measured needs to be homogeneous. One way to visualise the noise in the whole cross-section, not just inside ROIs, is to create a so-called noise map of the image. A noise map visualises how each voxel in the imaged volume is affected by random noise fluctuations [6]. This is done by scanning the same slice several times in order to measure the statistical variation of the signal in each voxel. As uniform, homogeneous phantoms were used in this thesis, this process was simplified by scanning the whole phantom and using successive images instead of performing several scans. Each voxel is assumed to be in the same position in all the images. By considering a given position in the image, the standard deviation of the CT numbers at this position is used to estimate the noise at this point in the image. This process is illustrated in Figure 3.10a. By calculating the noise in all the voxels in the image series, a noise map can be created. The creation of a noise map for the ATCM phantom is illustrated in Figure 3.10. The noise maps in this thesis were made using the open source software ImageJ (National Institutes of Health, USA) [34].

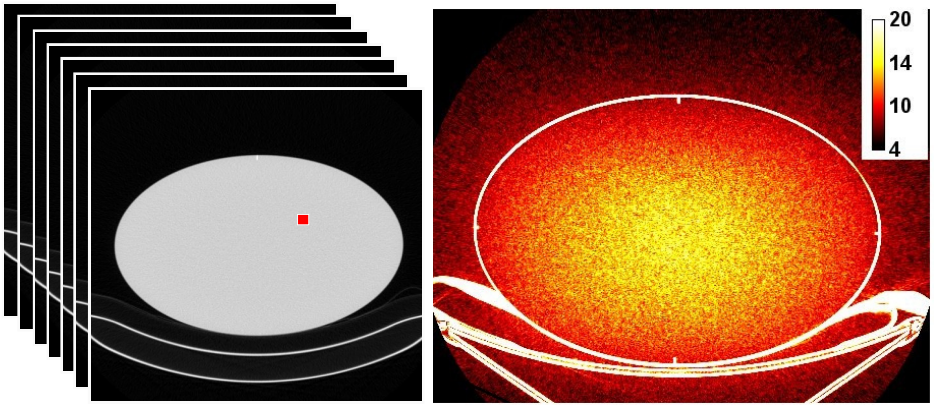

(a) (b)

Figure 3.10: (a) In order to make a noise map, the noise in a voxel (here marked in red) is measured. This is done by calculating the standard deviation of the pixel values of the same position in a series of images of the same object. (b) The resulting noise map, with a colour scale indicating the amount of noise in each voxel.

Chapter 4

Results

4.1 The CTDI phantom

The CTDI phantom was used for both dose and noise measurements, in order to compare the dose reduction and corresponding noise in specific areas.

4.1.1 Dose measurements

The relative doses measured when X-CARE was used compared to a standard scan, at different positions in the CTDI phantom, are shown in Figure 4.1. For the head phantom, the dose was reduced by 28 ± 3% in the North position, and with 19 ± 1% and 23 ± 3% in the North West and North East positions, respectively. The dose on the posterior (South West, South and South East) increased by 8-17%.

The changes in dose on the Siemens scanner were larger for the body phantom than for the head. In the North position the dose was reduced by 51 ± 6%, and with 19 ± 7% and 30 ± 10% in the North West and North East positions, respectively. The dose increase at the posterior was also higher than for the head, at 23-30%.

The relative doses when ODM was used compared to a standard GE scan are shown for the head and body CTDI phantom in Figure 4.2. In the head phantom, the dose was reduced by 16-18 ± 1% on the anterior (North East, North and North West). The dose reduction was small on the East and West positions, and in the South the dose was the same as for a standard scan.

The changes in the body phantom were larger than in the head phantom when ODM was used, where the dose was reduced by 37 ± 1% in the North position, and slightly less in the North West and North East positions. The dose reduction was 16-18% in the West and East positions, and in the South position the dose was the same as for a standard scan.

The DLP values for both the Siemens and GE scanner, as well as the relative dose changes for the head and body CTDI phantoms are listed in Appendix A.

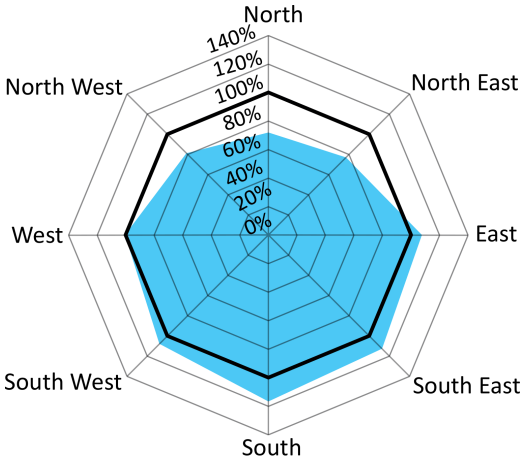

(a) Head 16 cm

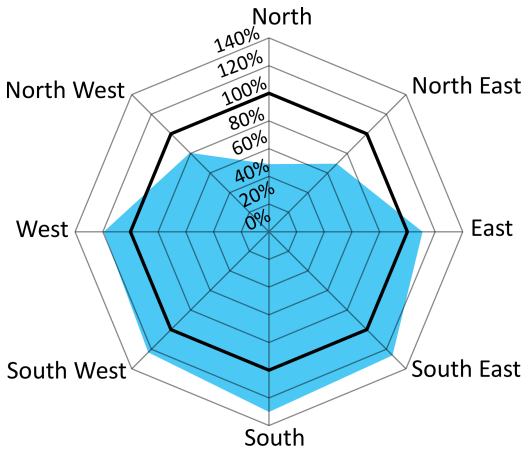

(b) Body 32 cm

Figure 4.1: The measured DLP for Siemens' X-CARE relative to a standard scan along the periphery of the phantom is shown in blue, for (a) the CTDI head phantom and (b) the CTDI body phantom. The thick line indicates the DLP measured for a standard Siemens scan.

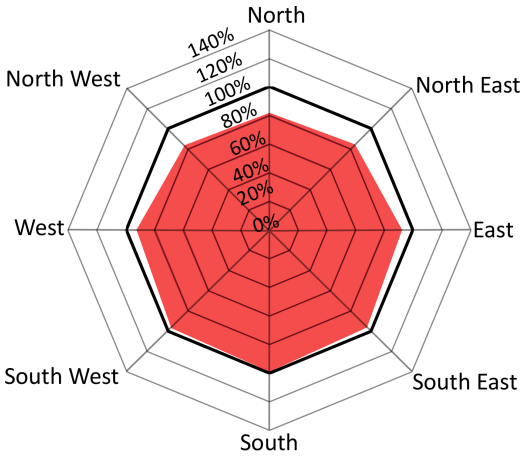

(a) Head 160 mm

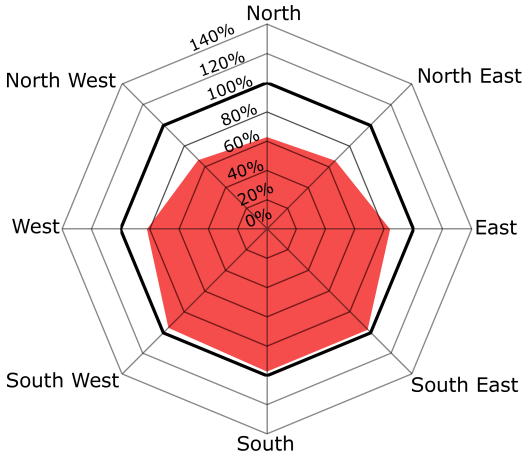

(b) Body 320 mm

Figure 4.2: The measured DLP for GE's ODM relative to a standard GE scan along the periphery of the phantom is shown in red, for (a) the CTDI head phantom and (b) the CTDI body phantom. The thick line indicates the DLP measured for a standard GE scan. The scales extend to 140% to allow a simpler visual comparison with X-CARE.

4.1.2 Noise in different ROIs in the CTDI phantom

Measurements of the noise in the CTDI head phantom for the Siemens scanner (see Table 4.1) indicate that there was a statistically significant ($p < 0.05$) increase of noise in the ROIs in the North, South and centre positions. This increase is very small, between 5% and 10%. No significant changes were found in the East and West positions.

In the CTDI body phantom (see Table 4.2) a significant ($p < 0.05$) noise increase was measured in the North and South positions, while a significant *decrease* was measured in the West position. These changes were very small, less than 10% from the noise level of the standard scan.

For both phantoms, the noise level was similar along the periphery of the phantoms, but increased in the middle, as expected, due to the lower dose.

For the GE scanner, a statistically significant increase of noise was measured in the North position of the head phantom (see Table 4.3), while a statistically significant *decrease* was measured in the West, East and centre positions. No change ($p = 0.11$) was found in the South position.

For the body phantom, a significant increase of noise was measured in the North, West, East and centre positions when ODM was used. No change ($p = 0.07$) was found in the South position. The measured noise levels in the CTDI body phantom for the GE scanner are shown in Table 4.4.

Table 4.1: Noise at different positions of the CTDI head phantom for a standard Siemens scan and a scan with X-CARE. The reported values are averages ± one standard deviation. The p-values indicate the likelihood of the standard and X-CARE scans having the same amount of noise.

Position	Noise standard scan [HU]	Noise X-CARE [HU]	p-value
North	3.2 ± 0.1	3.5 ± 0.1	$9.8 \cdot 10^{-4}$
East	3.4 ± 0.2	3.5 ± 0.1	0.065
South	3.4 ± 0.1	3.6 ± 0.3	$1.6 \cdot 10^{-4}$
West	3.5 ± 0.2	3.5 ± 0.1	0.36
Centre	3.9 ± 0.1	4.1 ± 0.3	$5.5 \cdot 10^{-4}$

Table 4.2: Noise at different positions of the CTDI body phantom for a standard Siemens scan and a scan with X-CARE. The reported values are averages ± one standard deviation. The p-values indicate the likelihood of the standard and X-CARE scans having the same amount of noise. *) The measured noise is significantly *lower* for X-CARE than for the standard scan.

Position	Noise standard scan [HU]	Noise X-CARE [HU]	p-value
North	23 ± 1	25 ± 1	$2.3 \cdot 10^{-6}$
East	23 ± 1	23 ± 1	0.052
South	24 ± 1	25 ± 2	$6.0 \cdot 10^{-4}$
West	23 ± 1	22 ± 1	$6.5 \cdot 10^{-4}$ *
Centre	32 ± 1	32 ± 2	0.13

Table 4.3: Noise at different positions of the CTDI head phantom for a standard GE scan and a scan with ODM. The reported values are averages ± one standard deviation. The p-values indicate the likelihood of the standard and ODM scans having the same amount of noise. *) The measured noise is significantly *lower* for ODM than for the standard scan.

Position	Noise standard scan [HU]	Noise ODM [HU]	p-value
North	3.8 ± 0.1	3.9 ± 0.2	0.0011
East	3.8 ± 0.2	3.6 ± 0.1	$3.8 \cdot 10^{-8}$ *
South	4.0 ± 0.1	3.9 ± 0.2	0.11
West	3.8 ± 0.2	3.6 ± 0.2	$1.7 \cdot 10^{-8}$ *
Centre	4.7 ± 0.2	4.5 ± 0.2	$4.7 \cdot 10^{-4}$ *

Table 4.4: Noise at different positions of the CTDI body phantom for a standard GE scan and a scan with ODM. The reported values are averages ± one standard deviation. The p-values indicate the likelihood of the standard and ODM scans having the same amount of noise.

Position	Noise standard scan [HU]	Noise ODM [HU]	p-value
North	13 ± 1	14 ± 1	$6.6 \cdot 10^{-8}$
East	13 ± 1	15 ± 1	$1.5 \cdot 10^{-6}$
South	15 ± 1	16 ± 1	0.074
West	13.5 ± 0.9	14 ± 1	0.016
Centre	21 ± 1	22 ± 2	$8.8 \cdot 10^{-4}$

4.1.3 Noise maps of the CTDI phantom

The noise maps of the CTDI head and body phantoms for a standard scan and with X-CARE are shown in Figure 4.3. The noise maps show a small increase of noise near the centre of the head phantom, especially in the North-South direction. This is consistent with the noise increase measured in the North, South and centre ROIs in the head phantom. In the noise maps of body phantom there are less visible changes, but a small increase of noise can be seen in the North and South near the periphery of the phantom. This is consistent with the increase of noise measured in ROIs at these positions.

In the noise maps of the CTDI head phantom in the GE scanner in Figure 4.4, a decrease of noise can be seen in the West and East positions, consistent with the measurements in Table 4.3. A band of slightly higher noise levels in the North-South direction can also be seen. The noise maps of the CTDI body phantom show that the amount of noise increases slightly when ODM is used, compared to the standard scan. This is consistent with the noise measurements in Table 4.4

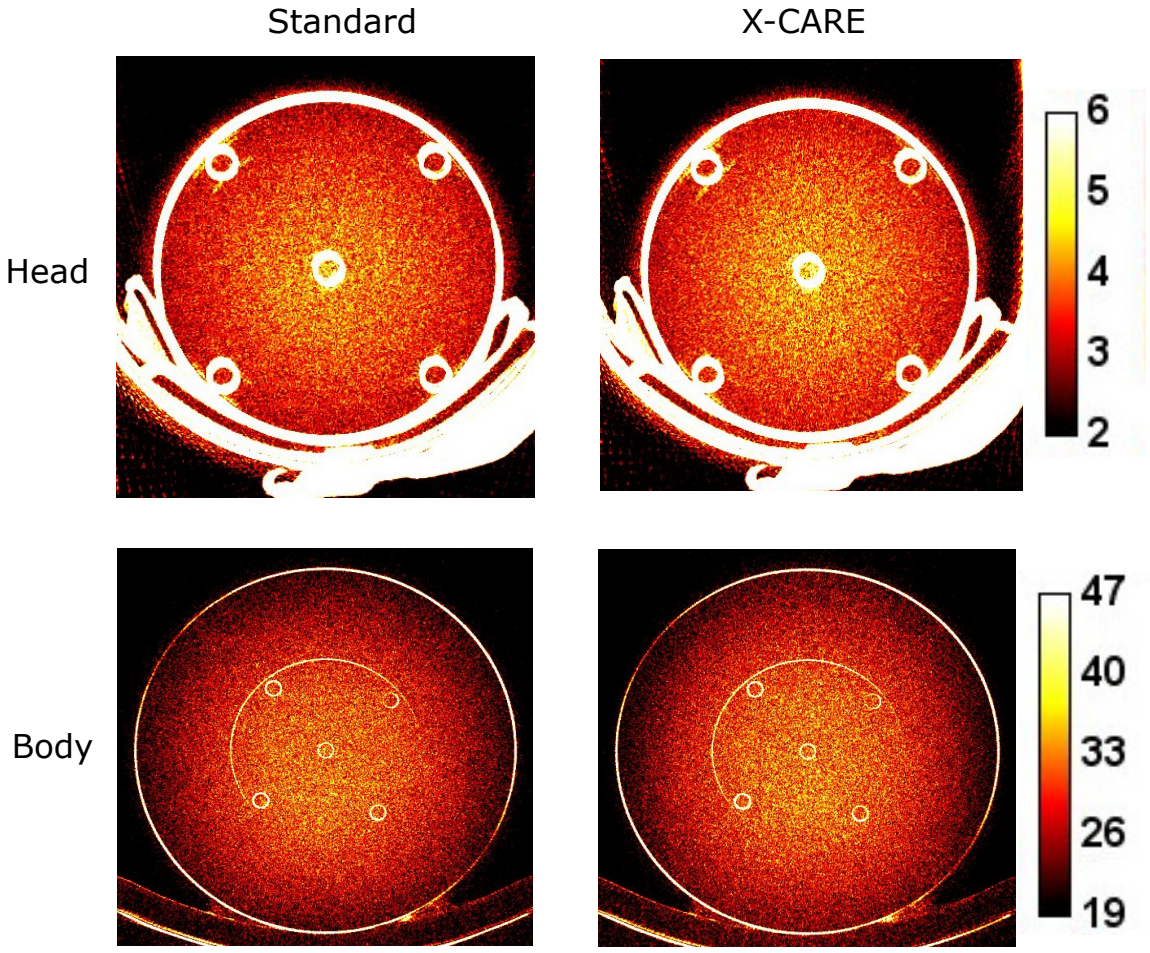

Figure 4.3: Noise maps of CT scans of the head and body CTDI phantom for a standard Siemens scan and a scan with X-CARE. Darker areas indicate less noise, and brighter areas indicate more noise, measured as the standard deviation between voxel values. The scale is in HU units. Each noise map is based on 38 images. The WL and WW are set so that the noise maps for the head and body phantom appear visually similar. The amount of noise is the same for the standard and X-CARE scans.

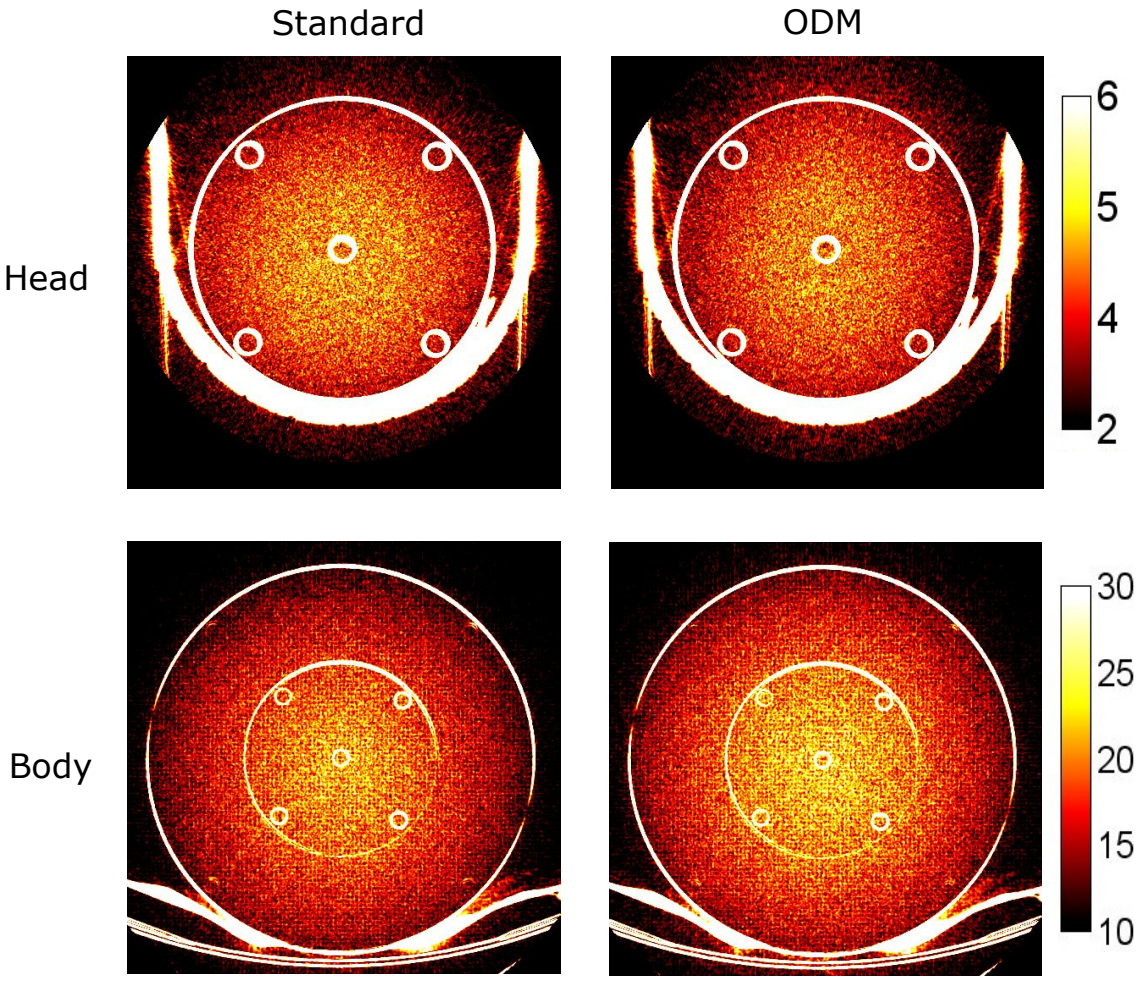

Figure 4.4: Noise maps of CT scans of the head and body CTDI phantom for a standard GE scan and a scan with ODM. The amount of noise appears to decrease slightly in the head phantom, and increase slightly in the body phantom. Darker areas indicate less noise, and brighter areas indicate more noise, measured as the standard deviation between voxel values. The scale is in HU. Each noise map is based on 38 images.

4.2 The ATCM phantom: the effect of different phantom sizes

The evaluation of the CTDI phantom showed that the doses are reduced when the OBTCM techniques are used, and that there are small changes in the image noise. The ATCM phantom allowed the effect of the phantom size on the OBTCM techniques to be examined.

4.2.1 Noise in the centre of the ATCM phantom

In the Siemens scanner, the amount of noise was found to increase with increasing phantom size. This was true both for the standard scan and the scan with X-CARE, as shown in Table 4.5. No significant difference in the amount of noise without and with X-CARE was measured for any of the different sizes ($p > 0.05$). The standard deviation of the noise was larger for X-CARE than for the standard scan, especially for the large section of the phantom.

Table 4.5: Average noise for a standard Siemens' scan and a scan with X-CARE. The noise was measured in a ROI in the centre of the ATCM phantom, and based on $N = 47$ images. The reported values are averages ± one standard deviation. The p-values indicate the likelihood of the standard and X-CARE scans having the same amount of noise. The amount of noise was the same ($p > 0.05$) for the two scans for a given size, but the noise level increased with phantom size.

Size	Noise standard scan [HU]	Noise X-CARE [HU]	p-value
Small	11.7 ± 0.4	11.9 ± 0.5	0.079
Large	16.6 ± 0.4	16.7 ± 0.7	0.48
Medium	14.1 ± 0.4	14.2 ± 0.6	0.33

In the GE scanner, the amount of noise was lower in the small section of the ATCM phantom than in the medium and large sections, both for the standard scan and the ODM scan. For all three sections, the amount of noise increased by approximately 10% when ODM was used ($p < 10^{-8}$). The mean values and standard deviations of the measured noise in the three sections are shown in Table 4.6. The standard deviations of the noise were generally higher for GE than for Siemens.

Table 4.6: Average noise for a standard GE scan and a scan with ODM. The noise was measured in a ROI in the centre of the ATCM phantom, and based on $N = 47$ images. The reported values are averages ± one standard deviation. The p-values indicate the likelihood of the standard and ODM scans having the same amount of noise. The amount of noise increased significantly ($p < 0.05$) in all three sections when ODM was used.

Size	Noise standard scan [HU]	Noise ODM [HU]	p-value
Small	12.9 ± 0.9	14.2 ± 0.9	$4.1 \cdot 10^{-10}$
Large	14.4 ± 0.7	15.8 ± 0.9	$1.1 \cdot 10^{-12}$
Medium	14.3 ± 0.8	15.6 ± 1.2	$9.7 \cdot 10^{-9}$

4.2.2 Noise maps of the ATCM phantom

The noise maps in Figure 4.5 support the measurements of the noise remaining constant when X-CARE is used. They also show that the amount of noise increased with the phantom size.

Figure 4.6 shows that for the GE scanner, the amount of noise was lower in the small section of the ATCM phantom than in the medium and large sections. Additionally, the noise maps illustrate the amount of noise increased slightly when ODM was used, compared to the standard scan.

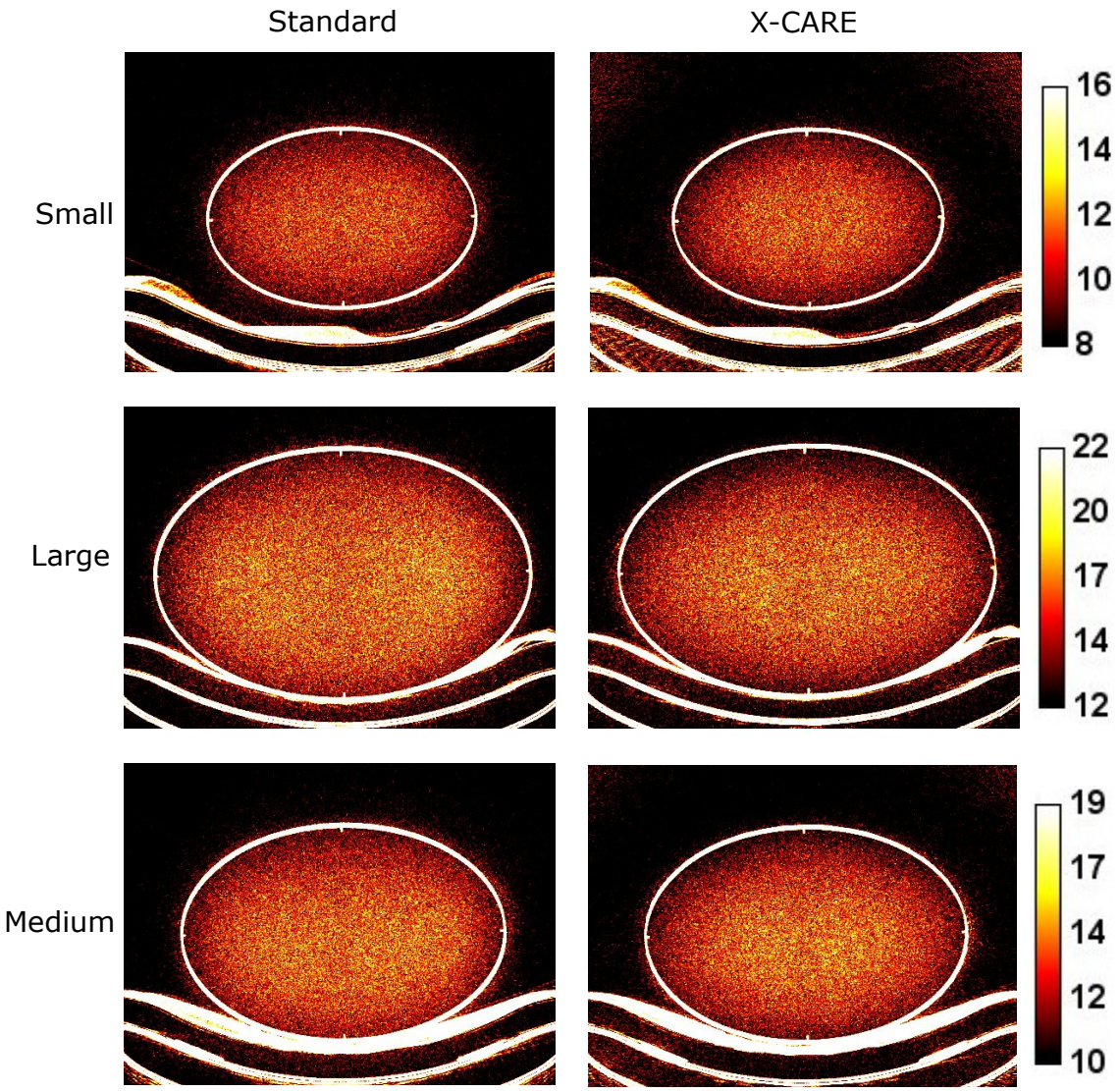

Figure 4.5: Noise maps of CT scans of the small, large, and medium sections of the ATCM phantom for a standard Siemens chest scan and a scan with X-CARE. Darker areas indicate less noise, and brighter areas indicate more noise, measured as the standard deviation between pixel values. The scale is in HU. The WL and WW are set so that the noise maps without X-CARE appear visually similar for the different sizes. The amount of noise is the same for the standard and X-CARE scan, but the amount of noise increases with phantom thickness. Each noise map is based on 47 images.

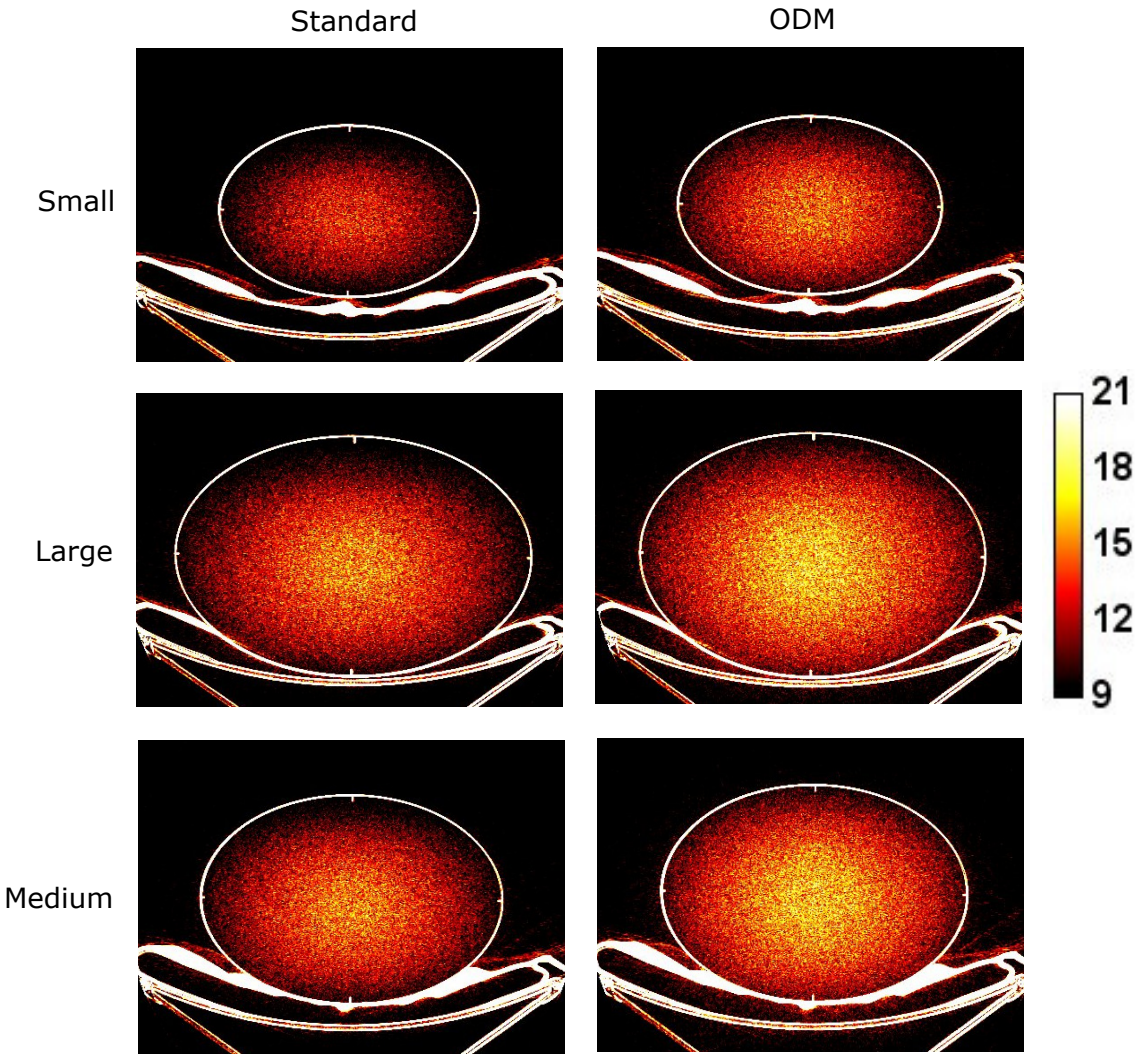

Figure 4.6: Noise maps of CT scans of the small, large, and medium sections of the ATCM phantom for a standard scan and a scan with ODM. The amount of noise increases slightly when ODM is used, as expected. Darker areas indicate less noise, and brighter areas indicate more noise, measured as the standard deviation between pixel values. The scale is in HU. The WL and WW are set to the same values in all the images because these values give a good illustration of the noise distribution for all the noise maps, as well as illustrating the small difference between the different sections. Each noise map is based on 47 images.

4.3 An alternative to OBTCM: reducing the tube current

X-CARE and ODM modulate the delivered dose. However, if these solutions were not available, an alternative approach to reducing dose to eye lenses and breasts would be to reduce the dose in the entire scan the way X-CARE and ODM reduce the dose in the anterior region. Doing this increased the amount of noise in the images, as shown in the noise maps in Figure 4.7, where the applied mAs was reduced by 40% in the noise maps with low mAs. Decreasing the mAs gave images with more noise than the OBTCM techniques.

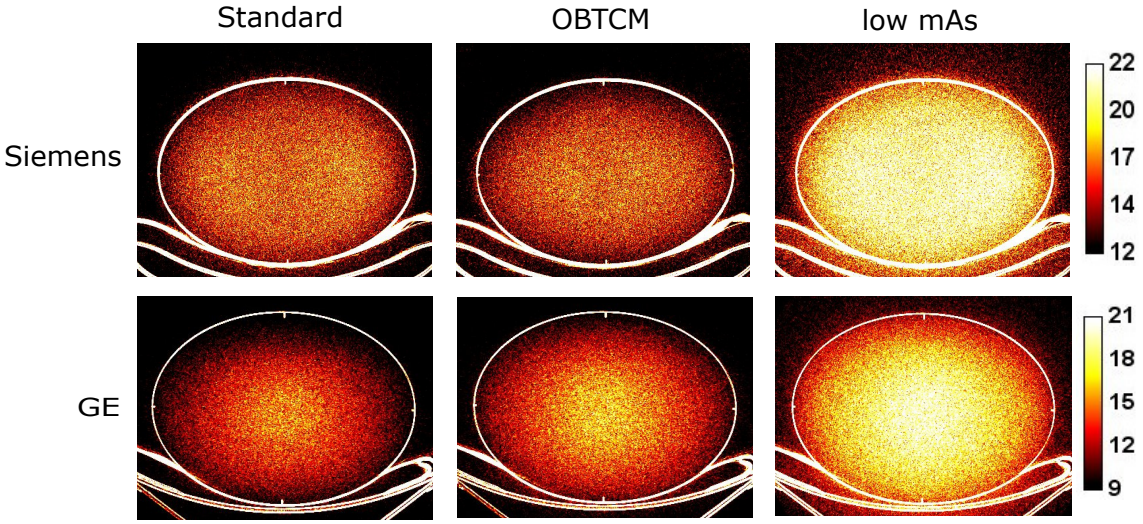

Figure 4.7: Noise maps for the large part of the ATCM phantom for an overall reduction of mAs compared to the standard scan and X-CARE/ODM techniques for Siemens and GE, respectively. As previously observed, X-CARE maintains the amount of noise, while it increases when ODM is used. As expected, the amount of noise increased when the mAs was reduced for both Siemens and GE compared to both the standard and OBTCM techniques. The scale is in HU, and each noise map is based on 47 images. Similar results were seen for the other phantom sizes.

A 40% reduction of mAs gives a 40% reduction of the delivered dose, and from Equation 2.11 approximately 30% increase in image noise was expected. The measured increase in image noise was approximately 30% for low mAs compared to a standard scan for the Siemens scanner (see Table 4.7), and 37-40% for the GE scanner (see Table 4.8).

The increase in noise when reducing the mAs was significant for both Siemens ($p < 10^{-50}$ for all sections) and GE ($p < 10^{-30}$ for all sections).

Table 4.7: Average noise in each slice measured in a ROI in the centre of the ATCM phantom with a 40% reduction of mAs for the Siemens scanner. The values for the standard scan and X-CARE are repeated for comparison. The values are the average noise measured in 47 images ± one standard deviation.

Size	Standard scan [HU]	X-CARE [HU]	Reduced mAs [HU]
Small	11.7 ± 0.4	11.9 ± 0.5	15.2 ± 0.5
Large	16.6 ± 0.4	16.7 ± 0.7	21.3 ± 0.5
Medium	14.1 ± 0.4	14.2 ± 0.6	18.1 ± 0.5

Table 4.8: Average noise in each slice measured in a ROI in the centre of the ATCM phantom with a 40% reduction of mAs for the GE scanner. The values for the standard scan and ODM are repeated for comparison. The values are the average noise measured in 47 images ± one standard deviation.

Size	Standard scan [HU]	ODM [HU]	Reduced mAs [HU]
Small	12.9 ± 0.9	14.2 ± 0.9	18.1 ± 0.3
Large	14.4 ± 0.7	15.8 ± 0.9	19.8 ± 0.2
Medium	14.3 ± 0.8	15.6 ± 1.2	19.6 ± 0.5

Chapter 5

Discussion

The two most central topics related to CT scans are patient dose and image quality, which are inextricably linked together. For images reconstructed only with FBP, a decrease in dose carries with it an increase in the image noise, but a *redistribution* of the patient dose does not have the same disadvantage. It is therefore possible to reduce the dose to certain body parts at the expense of others, without affecting the image quality.

Image quality can be measured in several different ways, each reflecting different qualities of the images. In this thesis image noise is the only indicator of image quality that is evaluated, due to it being straight-forward to quantify, and also that it is expected to be one of the indicators of image quality that is most affected by OBTCM techniques. A change in noise was considered significant if the significance level was below 0.05.

As OBTCM techniques alter the mAs during a scan, they directly affect both the patient dose and the amount of noise, both of which are central aspects of a CT scan. Like all other radiologic procedures, it is therefore important that the OBTCM techniques are optimised according to the ALARA principle. In addition, extra care must be taken to keep the sensitive organs within the area of dose reduction, both by positioning the patient correctly and by restricting the breast positions, lest the techniques counteract their purpose.

Siemens and GE have chosen different approaches to OBTCM, with Siemens aiming to maintain the image quality without reducing the total patient dose, while GE reduces the overall dose by allowing more image noise. It seems fitting to begin by evaluating the techniques in terms of how they affect the dose, both to the sensitive organs of interest and the total patient dose, and the noise of the resulting images.

5.1 Vendor differences

Apart from their common strategy of simply reducing the current when passing over a sensitive organ, Siemens and GE have fundamentally different approaches to their OBTCM techniques. A large portion of the work in radiography is to balance radiation dose and image quality. One may say that Siemens' philosophy focuses on image quality, while GE's philosophy focuses on the radiation dose. This is evident through Siemens aiming to keep the CTDI_{vol} constant when X-

CARE is applied, by increasing the tube current from the posterior, in order to maintain the image quality of a standard scan. The delivered dose is distributed differently, but the patient dose is the same as for a standard scan. GE, on the other hand, does not try to compensate for the anterior current reduction, and allows a reduction of both $CTDI_{vol}$ and image quality. This means that the reduced dose to the sensitive organs gives an overall patient dose reduction. The $CTDI_{vol}$ for the chest protocol was reduced by 20% when ODM was used, and with 10% for the head protocol. The results showed a 10% noise increase in the ATCM when the ODM chest protocol was used, as expected. This is a small change, that may not be visible clinically, but further studies should include an evaluation from a radiologist on whether the noise increase is clinically acceptable. The measurements of the head protocol (only used on the CTDI head phantom) showed a small decrease of noise in most of the ROIs, which is also supported by the noise maps. This indicates that the ODM head protocol does not increase the image noise.

The differences between X-CARE and ODM are largest for the chest protocol. X-CARE gives a larger dose reduction in the North position than ODM, whereas the breasts usually are located closer to the North West and North East positions, where the dose reduction is slightly larger for ODM than for X-CARE. This means that the dose to the breasts will be reduced by approximately the same factor for the two techniques. However, there is a trade-off for this reduction. X-CARE increases the dose on the posterior, which increases the dose to e.g. the spinal cord, and ODM increases the amount of noise by approximately 10%. These considerations must be weighed when deciding which technique is preferable.

5.2 Dose

Overall, the measured doses for X-CARE relative to a standard scan in Figure 4.1 are as expected. The dose is significantly reduced on the anterior of the phantom, and increased on the posterior. The difference between anterior and posterior is larger for the body phantom than for the head phantom, but the shape of the distribution is the same. The dose distribution matches Siemens' reported 120°sector of current reduction. The measured dose reduction at the North position of the body phantom was 51 ± 6%, which is slightly larger than the 30-40% reduction claimed by Siemens [35].

For GE, the measured doses for ODM relative to a standard scan in Figure 4.2 were as expected; reduced on the anterior and no change on the posterior of the phantom. The dose reduction on the anterior was larger for the body phantom than for the head phantom, as also was the case for X-CARE. However, the dose in the body phantom was also reduced considerably at the West and East positions. ODM's reported angular width of current reduction for the scanner used is 150° for the chest protocol, but the measured dose reduction covered at least 180°. This is likely due to a non-instantaneous current increase, so that the current starts increasing before the beam points towards the East and West positions, but has not yet reached its maximum value. This effect is still visible on the head phantom, but is smaller due to the smaller current reduction field of 90°, so that the tube current has almost reached its maximum by the time it passes over the East and West positions. ODM reduces the total patient dose relative to a standard scan.

Due to restrictions in the availability of the CT scanners, the number of dose measurements in this thesis was limited. Only three measurements were performed in each position, and this was deemed too few to perform statistical analysis and calculate p-values for the change. In spite of the low number of measurements, the data is assumed to be reasonably reliable, due to annual dose checks in the CTDI phantom performed by physicists at HUH and HDS. The physicists ensure

that the variation of dose between different scans stays well below 10%, much lower than the dose reductions measured in this thesis.

5.2.1 Differences between head and body OBTCM

One thing that the OBTCM techniques have in common is that the dose reduction in the anterior of the patient is considerably larger for the CTDI body phantom than for the head phantom. The difference was about 20 percentage points for both vendors (roughly 50% (body) vs 30% (head) dose reduction for X-CARE, and 40% (body) vs 20% (head) reduction for ODM). This is probably a direct consequence of the smaller dimensions of the head, or may be due to consideration not to increase the posterior current too much in a head scan, lest the back of the brain be exposed to too much radiation. The X-ray beam is attenuated less by the head phantom than by the body phantom due to the difference in size. This means that in the head phantom a projection from the posterior will contribute to the dose in the anterior to a larger degree than for the body phantom. This difference helps explain why the dose reduction on the anterior is smaller for the head phantom than for the body phantom.

The difference could be compensated for by having a larger difference between the anterior and posterior mAs for the OBTCM head protocol. This would, however, cause X-CARE to increase the dose delivered to the back of a patient's brain, which is not desirable. For ODM, a further decrease of mAs in the anterior gives both a lower anterior dose and a lower total dose. This causes a corresponding increase in image noise and degrades the image quality. It is therefore problematic to obtain a similar magnitude of dose reduction to the eyes as for the breasts.

5.2.2 Breasts outside the 120° field of dose reduction

Siemens and GE have different approaches to the size of the sector of dose reduction. Siemens reduces the dose in the anterior 120°, while increasing the dose in the remaining 240° for both the head and chest protocols. GE reduces the dose in the anterior 90° for the head protocol, and with 150° for the chest protocol, without an increase in the posterior dose. This means that there is a section of 15° on either side where the two scanners behave fundamentally different; Siemens increases the dose, and GE reduces it, relative to the standard scans. If the breasts are fully located within the 120° sector Siemens uses, this difference is negligible. However, if they are not, they will receive a higher dose when X-CARE is used than they would during a standard scan. For pre-teens and most early teens, this is not an issue, as their breasts are normally so small and firm that their positions are not affected much by the patient lying on their back. However, the breasts of young patients are particularly radiosensitive, especially during the period of breast development [2], so it is important to take extra care in the positioning.

For older teens and grown women the likelihood of breast "sagging" is very much present [36]. This is challenging because the outer breast region contains a higher percentage of glandular tissue, which makes it more susceptible to cancer [24]. Sagging breasts may not stay within a 120° field, or even within 180°. This means that a busty and/or old woman with free-hanging breasts is likely to receive a higher breast dose than if her breasts are within the sector of dose reduction.

Figure 4.1b shows that breasts sagging to the sides (East and West) would receive an approximately 20% higher dose with X-CARE than they would during a standard scan. This is a major challenge associated with OBTCM techniques [24].

For ODM (in Figure 4.2b) the breast dose for breasts in the West and East positions would

have been reduced by 20%, which is less than the maximum 40% reduction in the North position, but is still a notable reduction compared to the standard scan.

In order to make full use of chest OBTCM it is important to either restrict the use to young and/or flat-chested females, or to restrict the breast positions to within the desired angular section [24], e.g. by the wearing of a brassiere. An illustration of the effect of wearing a brassiere on a large-breasted female is shown in Figure 5.1. In a previous study, the wearing of a brassiere did not introduce any diagnostically relevant artifacts [36].

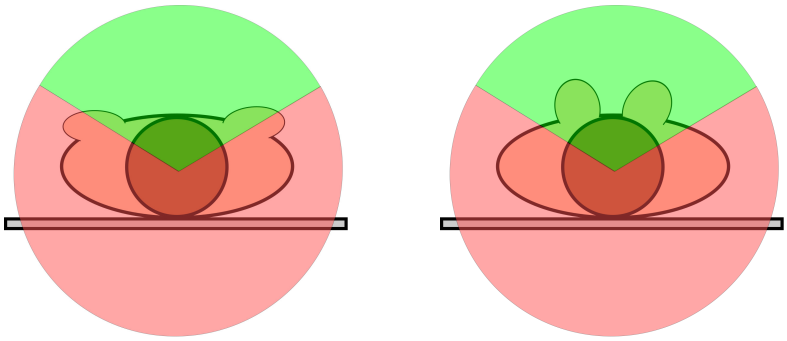

(a) Natural breast position (b) Restricted breast position

Figure 5.1: (a) Large and old breasts are more likely to sag sideways during a scan than small and young breasts. This may cause them to receive a higher dose (red) rather than the intended lower dose (green). (b) Restricting the breasts' position with e.g. a brassiere aids in keeping them within the area where they receive a lower dose from the OBTCM technique.

5.2.3 The importance of correct vertical positioning

As both OBTCM techniques reduce the current in an angular section, the vertical patient positioning is especially important when these techniques are used. For the sensitive organs to benefit from the OBTCM, they must be within the area where the current is reduced. It is then important to position the patient at the isocentre. However, patients are often centred too low in the gantry [37], which reduces the proportion of the patient in the current-reduced zone. Positioning at and below the isocentre and the effects on the dose to the breasts in the case of X-CARE are illustrated in Figure 5.2.

The eyes are located closer to the North direction than the breasts, and are directly exposed to a narrower range of radiation angles. This means that too low positioning is more likely to affect the breast dose than the dose to the eye lenses.

For ODM a low positioning will reduce the effect of the current reduction, as a larger part of the patient is irradiated as for the standard scan. For X-CARE, which *increases* the current in the lower part of the rotation, a low positioning means that the patient is exposed to a *higher* dose than during a standard scan, and may also increase the dose to the sensitive areas [37].

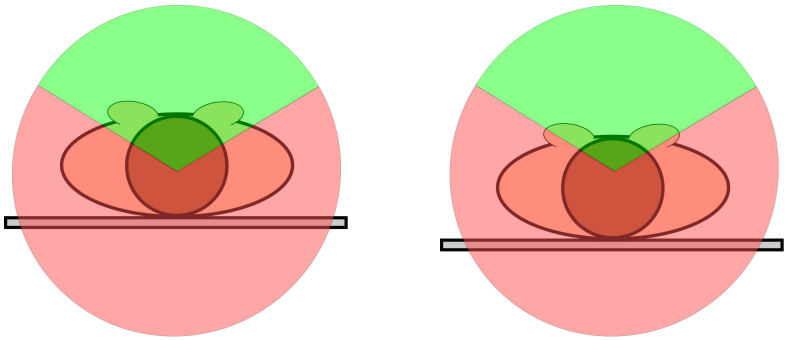

(a) Positioning at the isocentre (b) Low positioning

Figure 5.2: Vertical positioning is important when OBTCM techniques are used, especially if the current is increased on the posterior. The dose-reduced sector of X-CARE is shown in green. (a) The patient is correctly positioned at the isocentre and the breasts are within the sector of reduced dose. (b) The patient is positioned too low, and the breasts are (partly) outside the current-reduced zone and even receive a higher dose than during a standard scan.

5.3 Noise

The performed noise measurements are in line with the claims made by Siemens that X-CARE reduces the dose to sensitive organs without compromising the image quality [35]. For Siemens this means that there was no increase in noise when X-CARE was used compared to a standard scan, due to a redistribution of dose that kept the detector dose constant, as illustrated in Figure 3.4.

When the total patient dose is reduced, as it is when ODM is used, an increase in image noise is expected. The measurements in this thesis show that the amount of noise increased slightly when ODM was used, as expected.

5.3.1 Noise in the CTDI phantom

Siemens

The measurements in small, circular ROIs in the CTDI phantom indicated that the amount of noise increased slightly (less than 10%) in the North-South direction for both the head and body phantom. Although the increase was mathematically significant, it may not be visible to a radiologist evaluating the images. The differences between the average amounts of noise without and with X-CARE in Tables 4.1 and 4.2 are of the same order as the standard deviation of the noise within a scan. This means that the difference between the standard scan and X-CARE is comparable to the difference between different image slices in the same scan. In addition, the ROIs used in this phantom are relatively small, and the measured differences are not necessarily representative for the rest of the phantom.

In the noise maps of the CTDI phantoms in Figure 4.3, a slight increase of noise can be seen along the North-South direction when X-CARE is used, as well as a slight decrease in the East-West direction. Since X-CARE increases the tube current for 240°, including from the East and West,

these projections give a higher dose and a higher detector signal than the North-South projections, and therefore less noise.

The North-South noise band is more visible in the head phantom than in the body phantom. The difference between the head and body may be due to the body noise maps having a larger WW than the head, so that small differences are less visible. It is worth noting that the ROIs along the periphery of the phantoms (especially in the North and South positions) are placed in the areas where the difference between the standard and X-CARE noise map are the largest. That is, the noise increase measured in the ROIs represent the largest difference between the standard Siemens scan and X-CARE. The overall impression from the noise maps is that the amount of noise without and with X-CARE is very similar. This highlights the advantage of considering noise maps when evaluating image noise. Although they are a visualisation tool more than they provide numbers and uncertainties, they are not limited to arbitrarily positioned ROIs, but provide insight in all positions. The disadvantage is that in order to create them, one needs either a uniform phantom or to scan the same slice of a non-uniform object a large number of times.

GE

From Table 3.3, the CTDI_{vol} was reduced by about 10% when ODM was used on the head phantom. This corresponds to an expected noise increase of about 5%. For the body phantom, the CTDI_{vol} was reduced by about 20%, corresponding to a noise increase of 11%. This means that the noise is expected to increase more in the body phantom than in the head phantom.

The measurements in the ROIs in the CTDI head phantom in Table 4.3 showed a slight decrease of noise in the East, West and centre positions, with no change in the South position, and a slight increase in the North position. The same trend can be seen in the noise maps in the upper part of Figure 4.4, where the noise in the ODM scan is slightly reduced compared to the standard scan. The noise maps also show a band of noise in the North-South direction for ODM, while the noise in the standard scan is more symmetric around the centre of the head phantom. This band of noise is due to the lower mAs in the upper 90° of the X-ray tube rotation. The projections in the North-South direction contribute with a lower detector dose and therefore higher amount of noise than the projections in the East-West direction. However, it is surprising that a decrease of noise is seen, and not just an increase of noise in a band along the North-South direction. It is possible that this is due to the way the images are reconstructed with GE; there is a small contribution from iterative reconstruction in the FBP, which may skew the data from what is expected from pure FBP.

The results match the expected noise increase better for the CTDI body phantom (see Table 4.4). A significant increase ($p < 0.05$) of noise was measured in all ROIs except in the South position (where $p = 0.07$). The increase was small; of order 5-15%. This is in agreement with the expected 11% noise increase. The same trend was seen in the noise maps of the body phantom in the bottom part of Figure 4.4, where the amount of noise increases slightly everywhere in the phantom. However, even though the noise increase was measured and is visible on the noise maps, the difference may not be visible to a radiologist in a clinical setting.

5.3.2 Noise in the ATCM phantom

The ROI used in the ATCM phantom was much larger than those used in the CTDI phantom, and is therefore better suited to quantify the changes in noise. Also, the different sections of the ATCM phantom allow the two scanners' response to different patient sizes to be examined.

Siemens

In Table 4.5 there is no significant change ($p > 0.05$) in the amount of noise when X-CARE is used compared to the standard scan, for any of the sections. This is consistent with Siemens' claim, and with the similar CTDI_{vol} for the two scans (see Table 3.2). The amount of noise increases as the phantom size increases. Larger patients tend to have more inter-organ fat, which acts as a natural contrast agent and makes it easier to distinguish organs. In addition, there is more space between the organs of a large patient, meaning that a higher level of noise can be tolerated while still producing clinically acceptable images. The noise maps in Figure 4.5 also support the measurements of the amount of noise being equal for the standard scan and for X-care, and that the noise increased with the phantom size.

X-CARE had a slightly larger variation in measured noise than the standard scan (a higher standard deviation), which may be due to the current modulation creating a radiation field which is less homogeneous than the one sketched in Figure 2.7b.

GE

According to Table 4.6 there was a significant increase in noise of about 10% when ODM was used compared to the standard scan. This is in line with the expectation of an 11% increase based on the CTDI_{vol} of the two scans, and the noise measured in the CTDI phantom.

Notably, the amount of noise was the same for the medium and large section, while it was lower in the small section of the ATCM phantom. The GE scanner seems to react differently to differently sized patients than the Siemens scanner did. The GE scanner aims to keep the amount of noise the same in each image slice, regulated by a noise index setting on the scanner. It also appears to try to keep the amount of noise similar for patients of different sizes, except for very thin patients. This adjustment, which reduces the noise in the thinnest patients, is probably necessary due to the limited space between organs and lack of inter-organ fat.

The standard deviation of the measured noise was higher for GE than for Siemens. This was due to an unknown feature of the reconstruction of 3 mm image slices in the GE scanner. Tests showed that this effect does not affect the amount of noise increase from the standard scan to the ODM scan, nor the significance of the increase.

The noise maps in Figure 4.6 support the claim of a small increase of noise when ODM is used, as well as the amount of noise being lower in the small section than in the medium and large sections.

5.4 An alternative to OBTCM: reducing the tube current

As an alternative to the OBTCM techniques, CT scans with global current reduction of 40%, comparable to the anterior current reduction of the OBTCM techniques, were examined. This resulted in an increase in image noise of about 30% for Siemens, in accordance with Equation 2.11 (compared to no change when X-CARE was used), and of 37-40% for GE (compared to an increase of about 10% when ODM was used). An increase in noise is expected when the global tube current was reduced, but the measured increase in noise for GE was larger than the expected 29% from Equation 2.11. The reason for this discrepancy is unknown. However, in spite of an attempt to only use images reconstructed with FBP, GE includes a small contribution from iterative reconstruction in their FBP algorithm, which cannot be removed by users of the scanner. This may cause some

variation in image noise that cannot be explained from Equation 2.11. The previously mentioned reconstruction to 3 mm slice thickness may also have contributed to the discrepancy.

The global tube current reduction must be assumed to be an unrealistic alternative. The dose reduction to the sensitive organs is approximately the same as when OBTCM techniques are used, but the images contain a much larger amount of noise. If such a large decrease of dose produces images which are clinically acceptable, the protocol of the standard scans should already have been changed to a lower mAs, according to the ALARA principle. It is assumed that HUH and HDS follow this principle, and a further reduction of mAs degrades the image quality beyond the acceptable.

Compared to the low-mAs images, the OBTCM images contained less noise, showing that OBTCM techniques do a better job than the simpler approach of reducing the tube current globally. The redistribution of dose allow to a large degree the image quality to be conserved while providing the same dose reduction to the sensitive organs. The comparison between OBTCM and global tube current reduction showcase that OBTCM techniques can be important tools in optimising CT scans.

5.4.1 An alternative to OBTCM and global current reduction: bismuth shielding

Bismuth shields have been used in CT imaging as a means of shielding radiosensitive superficial organs such as the eye lenses and breasts. This is done by placing a physical shield over the organ to be shielded, such that the primary radiation beam is attenuated by the shield before reaching the patient [38]. A major concern of using bismuth shields is that they can cause artifacts, increase noise and give inaccurate CT number values. In addition, some scanners must be "tricked" into not increasing the tube current during the scan to compensate for the additional attenuation of the shielding, by adding the shielding after the CT radiograph [2]. However, several studies [2, 38] have shown that globally decreasing the tube current provides the same organ dose reduction as bismuth shielding, while also decreasing the total patient dose. In addition, a global current reduction maintained a similar level of image noise as the bismuth shielding, but without the associated artifacts [2, 38]. This thesis has therefore only included a comparison with a global current reduction, as the bismuth shielding was deemed obsolete.

5.5 Clinical use

At HUH, X-CARE is used in head scans for patients of all ages. However, the X-CARE chest protocol is only used for pediatric patients (up to an age of 18). If extra care is taken in the patient centring, and the patient's breasts are supported by e.g. a brassiere, the use of X-CARE could be extended to include adult patients.

At HDS, the ODM chest protocol is used, while the ODM head protocol is not. When the GE scanner was installed, the radiologists were not satisfied with the image quality of head scans, and turning ODM off was among the changes that were made to the protocol. There has been no evaluation from radiologists there on whether there is a difference in image quality between a standard head scan and a head scan with ODM. The results in this thesis indicate that there is no increase in noise for the head scan, and at the very least it is expected to be smaller than for the chest scan. The low image quality the radiologists observed is therefore unlikely to stem from ODM, and HDS should consider using the technique on patients.

5.6 Limitations

In this thesis image noise was used as the only indicator of image quality. This is the most relevant parameter to consider when the dose is reduced, but other parameters could possibly contribute to a deeper understanding. Contrast-to-noise ratio (CNR) is a parameter that is often used in CT image evaluation [39], but as the phantoms used in this thesis are uniform, it was not possible to calculate the CNR. The noise measurements were restricted to uniform areas and can therefore only say something about how the OBTCM techniques affect the noise inside homogeneous areas of a patient.

Noise maps can be useful, but a disadvantage may be that they can be difficult to interpret. A "bright" pixel, meaning that the pixel has a (relatively) large variation in value between different slices, can have two possible explanations. It can mean that the pixel is in a noisy area, but it can also mean that there happens to be a large variation in signal between the different slices, without this necessarily meaning that there is much noise in the area within any individual image slice. Such a variation in the signal may be due to e.g. variations in the number of projections stemming from the value of the pitch (illustrated in Figure 2.7).

A large limitation of this thesis is that only uniform phantoms are used in the measurements, phantoms without the organs that the OBTCM techniques aim to reduce the dose to. This makes it difficult to say for sure that the eye lenses and breasts are within the areas that receive a lower dose when the OBTCM techniques are used. Further studies should include an anthropomorphic phantom, and dose maps showing a Monte Carlo-simulated distribution of dose throughout the body. The effect of the vertical positioning of the phantom on the dose distributions should also be examined further.

When the dose is measured in a CTDI phantom, the measurements are usually performed during an axial scan, i.e. one slice is scanned at a time, as opposed to a helical scan. The dose measurements in this thesis were performed during helical scans, as it was not possible to perform axial scans with OBTCM. In addition, the area to be scanned had to be selected manually, so it was challenging to select only one slice at the centre of the phantom. However, the same selected area was scanned without and with OBTCM, so the relative doses in Figures 4.1 and 4.2 are unaffected by the selected area, and the selected area was kept constant for a given scanner and given phantom, so that the DLP values without and with OBTCM within each table in Appendix A can be compared.

The 45° rotation of the CTDI phantoms used to measure the dose in the North West, North East, South East and South West positions was likely not exactly 45° because the position was determined from a visual inspection. However, both the standard and OBTCM scans were performed without moving the phantom, so the measurements of dose in Figures 4.1 and 4.2 are performed in the same phantom positions. The East-West asymmetry in the dose measurements may in part be due to deviations from the desired 45° rotation. The angular uncertainty also contributes to the difficulty in determining if the eye lenses and breasts are included in the sector of current reduction.

Of the two protocols in this thesis, the chest protocol was examined more thoroughly than the head protocol, as the head protocol was only used in the scanning of the CTDI head phantom, while the chest protocol was used for both the CTDI body phantom and the ATCM phantom. This was a natural consequence of the phantoms used.

Finally, the statistical analysis of image noise in this thesis was performed by using a t-test. For small sample sizes, this test is only appropriate if the data are normally distributed. However, this may not be the case for average noise levels, as noise values (standard deviations) are typically not normally distributed [3].

Chapter 6

Conclusion

In this thesis, the organ-based tube current modulation techniques X-CARE from Siemens and ODM from GE were compared and evaluated in terms of how the different techniques affected the image noise and radiation dose to the eye lenses and breasts, relative to standard CT scans.

X-CARE had a slightly larger dose reduction ($-28 \pm 3\%$) in the North position of the head scan than ODM ($-18 \pm 1\%$), but for the chest scan the dose reduction was similar where the breasts are often located (North West and North East positions).

The dose is reduced in different angular sections for X-CARE and ODM. The narrow section of 120° used in X-CARE chest scans make patient positioning crucial. The use of breast support (e.g. a brassiere) during scanning could help optimise the dose reduction to the breasts.

Siemens and GE have chosen different approaches to OBTCM. X-CARE maintains the amount of noise in the standard scan by redistributing the patient dose from the anterior to the posterior, which increases the dose to e.g. the spinal chord. ODM reduces the overall patient dose and allows an increase of image noise. However, an increase was only measured for the chest scan, not for the head scan. Suggestions were made for improving the head scan protocol at HDS.

Examination of the ATCM phantom showed that Siemens allows a larger amount of noise in large patients than in small patients. For a given size, the amount of noise is the same for the standard scan and for X-CARE. The noise maps support this. The noise in the GE images was less dependent on patient size than for Siemens, but the noise was reduced in the phantom size corresponding to the thinnest patient. The noise increases by about 10% in the ODM chest scans relative to the standard scan. An increase was also observed in the corresponding noise maps. Although this difference is mathematically significant, it may not be of clinical importance. Evaluation by radiologists is needed to assess if the image quality deteriorates noticeably when ODM is used on chest scans.

Bibliography

[1] A. Almén, E. G. Friberg, A. Widmark, and H. M. Olerud, "Radiology in Norway anno 2008. Trends in examination frequency and collective effective dose to the population.," tech. rep., Østerås: Norwegian Radiation Protection Authority, 12 2010.

[2] J. Wang, X. Duan, J. A. Christner, S. Leng, L. Yu, and C. H. McCollough, "Radiation dose reduction to the breast in thoracic CT: Comparison of bismuth shielding, organ-based tube current modulation, and use of a globally decreased tube current," *Medical Physics*, vol. 38, no. 11, pp. 6084–6092, 2011.

[3] J. Wang, X. Duan, J. A. Christner, S. Leng, K. L. Grant, and C. H. McCollough, "Bismuth shielding, organ-based tube current modulation, and global reduction of tube current for dose reduction to the eye at head CT," *Radiology*, vol. 262, no. 1, 2012.

[4] Oxford English Dictionary, "Tomography," 2019. [Online]. Available: `http://www.oed.com/view/Entry/203123` (Visited 01.03.2019).

[5] T. M. Buzug, *Computed tomography : from photon statistics to modern cone-beam CT*. Berlin: Springer, 2008.

[6] M. A. D. Guleng, "Radiation dose and image quality in CT- evaluation of how slice thickness, tube current modulation and reconstruction algorithms affect radiation dose and image noise," Master's thesis, NTNU, Norway, 2018.

[7] N. B. Smith and A. Webb, *Introduction to medical imaging : physics, engineering and clinical applications*. Cambridge texts in biomedical engineering, Cambridge: Cambridge University Press, 2011.

[8] N. Tomic, P. Papaconstadopoulos, S. Aldelaijan, J. Rajala, J. Seuntjens, and S. Devic, "Image quality for radiotherapy ct simulators with different scanner bore size," *Physica Medica*, vol. 45, pp. 65–71, 2018.

[9] C. C., J. DeMarco, E. Angel, and M. McNitt-Gray, "Estimating patient radiation dose from computed tomography." Cagnon - ACMP - Handout, 2008. [Online]. Available: `https://www.aapm.org/meetings/amos2/pdf/34-9723-93678-499.pdf` (Visited 03.06.2019).

[10] R. Deych and E. Dolazza, "New trends in X-ray CT imaging," *NATO Security through Science Series B: Physics and Biophysics*, pp. 15–35, 2006.

[11] N. Hamada, "Ionizing radiation sensitivity of the ocular lens and its dose rate dependence," *International Journal of Radiation Biology*, vol. 93, no. 10, pp. 1024–1034, 2017.

[12] E. J. Hall and A. J. Giaccia, *Radiobiology for the radiologist*. Philadelphia, Pennsylvania: Lippincott Williams & Wilkins, 6th ed., 2006.

[13] Siemens, "Simulation of x-ray spectra." [Online], Available at `https://www.oem-xray-components.siemens.com/x-ray-spectra-simulation`. Visited 21.02.2019.

[14] L. Goldman, "Principles of CT: Multislice CT*," *Journal of Nuclear Medicine Technology*, vol. 36, no. 2, pp. 57–68; quiz 75–6, 2008.

[15] C. H. McCollough, M. R. Bruesewitz, and J. M. Kofler, "CT dose reduction and dose management tools: overview of available options," *Radiographics : a review publication of the Radiological Society of North America, Inc*, vol. 26, no. 2, 2006.

[16] M. Söderberg and M. Gunnarsson, "Automatic exposure control in computed tomography – an evaluation of systems from different manufacturers," *Acta Radiologica*, vol. 51, no. 6, pp. 625–634, 2010.

[17] D. Merzan, P. Nowik, G. Poludniowski, and R. Bujila, "Evaluating the impact of scan settings on automatic tube current modulation in CT using a novel phantom," *British Journal Of Radiology*, vol. 90, no. 1069, 2016.

[18] J. Bryant, N. Drage, and S. Richmond, "CT number definition," *Radiation Physics and Chemistry*, vol. 81, no. 4, 2012.

[19] J. Altenbernd, A. Wetter, M. Forsting, and L. Umutlu, "Dual-energy CT of liver metastases in patients with uveal melanoma," *European Journal of Radiology Open*, vol. 3, pp. 254–258, 2016.

[20] S. A. Kane, *Introduction to physics in modern medicine*. London: Taylor & Francis, 2003.

[21] H. D. Nagel, *CT Parameters that Influence the Radiation Dose*, pp. 51–79. Berlin, Heidelberg: Springer Berlin Heidelberg, 2007.

[22] W. R. Hendee and M. K. O'Connor, "Radiation risks of medical imaging: separating fact from fantasy," *Radiology*, vol. 264, no. 2, 2012.

[23] M. Oseberg, V. Tran, K. Hoang, H. Lauvhaug, and H. T. P. Nguyen, "CT thorax lavdose - en sammenligning av et organdosemodulerings program X-CARE og vismut beskyttelse," *Radiography Open*, vol. 3, no. 1, pp. 10–10, 2017.

[24] W. Fu, X. Tian, G. M. Sturgeon, G. Agasthya, W. P. Segars, M. M. Goodsitt, E. A. Kazerooni, and E. Samei, "CT breast dose reduction with the use of breast positioning and organ-based tube current modulation," *Medical Physics*, vol. 44, no. 2, pp. 665–678, 2017.

[25] B. H. Østerås, K. Jensen, H. K. Andersen, and A. C. T. Martinsen, "Radiation-induced cataracts," *Tidsskrift for den Norske laegeforening : tidsskrift for praktisk medicin, ny raekke*, vol. 136, no. 21, 2016.

[26] D. Völgyes, *Image quality in forensic CT imaging*. PhD thesis, NTNU, Trondheim, 2018.

[27] K.-P. Chang, T.-K. Hsu, W.-T. Lin, and W.-L. Hsu, "Optimization of dose and image quality in adult and pediatric computed tomography scans," *Radiation Physics and Chemistry*, vol. 140, pp. 260–265, 2017.

[28] M. Diwakar and M. Kumar, "A review on CT image noise and its denoising," *Biomedical Signal Processing and Control*, vol. 42, pp. 73–88, 2018.

[29] P. Sprawls, "Computed tomography image quality optimization and dose management." [Online]. Available `http://www.sprawls.org/resources/CTIQDM/#32`. Visited 19.02.2019.

[30] The Phantom Laboratory, *CCT228 ATCM Phantom Manual*, 2017.

[31] M. Hammer, "X-ray physics: X-ray interaction with matter and attenuation." [Online], Available at `http://xrayphysics.com/attenuation.html`. Visited 08.05.2019.

[32] M. Khatonabadi, T. Hall, I. Boechat, S. Muir, C. Cagnon, M. McNitt-Gray, S. Borgheian, and M. Woo, "Reducing radiation exposure in pediatric CT- a shared responsibility." Quality Story Board, 96th Scientific Assembly and Annual Meeting of the Radiological Society of North America (RSNA); Chicago, Illinois. 2010.

[33] E. Wasbø, "ImageQC. quality control in medical imaging." [Online]. Available: `https://github.com/EllenWasbo/ImageQC` (Visited 12.03.2019).

[34] W. S. Rasband, "ImageJ." National Institutes of Health, [Online]. Available: `https://imagej.nih.gov/ij/` (Visited 12.03.2019).

[35] A. Krauss and B. Schmidt, "CARE Dose4D, X-CARE and CARE kV." Siemens Healthineers GmbH, October 2017.

[36] A. Seidenfuss, A. Mayr, M. Schmid, M. Uder, and M. M. Lell, "Dose reduction of the female breast in chest CT," *AJR. American journal of roentgenology*, vol. 202, no. 5, 2014.

[37] N. Lai, T. Chen, Y. Tyan, and H. Tsai, "Off-centre effect on dose reduction to anterior surfaces with organ-based tube-current modulation," *Radiation Measurements*, vol. 59, pp. 155–159, 2013.

[38] J. Wang, X. Duan, J. A. Christner, S. Leng, K. L. Grant, and C. H. McCollough, "Bismuth shielding, organ-based tube current modulation, and global reduction of tube current for dose reduction to the eye at head CT," *Radiology*, vol. 262, no. 1, 2012.

[39] J. Silkwood, K. Matthews, and P. Shikhaliev, "Tu-e-217bcd-04: Spectral breast CT: Effect of adaptive filtration on CT numbers, CT noise, and CNR," *Medical Physics*, vol. 39, no. 6Part24, pp. 3914–3914, 2012.

Appendix A

Dose tables

Tables A.1 and A.2 show the measured DLP for a standard Siemens scan and a scan with X-CARE, as well as the relative change between the scans, for the head and body CTDI phantom, respectively. Tables A.3 and A.4 show the same information for the scans without and with ODM.

Table A.1: Average DLP in the CTDI head phantom for a standard Siemens scan and a scan with X-CARE. The values are the average of three measurements ± one standard deviation, reported with one significant digit in the standard deviation. The relative change shows the difference between the standard and X-CARE scans.

Position	DLP standard scan [mGy·cm]	DLP X-CARE [mGy·cm]	Relative change
North	113 ± 4	81.0 ± 0.3	−28 ± 3%
North East	114.6 ± 0.6	88 ± 3	−23 ± 3%
East	106 ± 3	114 ± 5	+8 ± 5%
South East	110 ± 4	123 ± 5	+13 ± 6%
South	112 ± 3	131 ± 5	+17 ± 6%
South West	115 ± 3	124 ±1	+8 ± 3%
West	109 ± 3	109 ± 3	0 ± 4%
North West	108 ± 2	87.5 ± 0.9	−19 ± 1%
Centre	105.17 ± 0.06	110 ± 2	+5 ± 2%

Table A.2: Average DLP in CTDI body phantom for a standard Siemens scan and a scan with X-CARE. The values are the average of three measurements ± one standard deviation, reported with one significant digit in the standard deviation. The relative change shows the difference between the standard and X-CARE scans.

Position	DLP standard scan [mGy·cm]	DLP X-CARE [mGy·cm]	Relative change
North	33 ± 3	16 ± 1	−51 ± 6%
North East	34 ± 3	24 ± 3	−30 ± 10%
East	33 ± 3	37 ± 2	+11 ± 11%
South East	29 ± 3	37 ± 4	+26 ± 18%
South	29 ± 3	38 ± 3	+30 ± 15%
South West	29 ± 3	35 ± 2	+23 ± 15%
West	33 ± 3	39 ± 4	+19 ± 15%
North West	34 ± 3	27 ± 1	−19 ± 7%
Centre	16.6 ± 0.1	16.8 ± 0.3	+1 ± 2%

Table A.3: Average DLP in CTDI head phantom for a standard GE scan and a scan with ODM. The values are the average of three measurements ± one standard deviation, reported with one significant digit in the standard deviation. The relative change shows the difference between the standard and ODM scans.

Position	DLP standard scan [mGy·cm]	DLP ODM [mGy·cm]	Relative change
North	332 ± 4	271.2 ± 0.3	−18 ± 1%
North East	330 ± 2	278 ± 3	−16 ± 1%
East	319 ± 5	295 ± 3	−7 ± 2%
South East	317 ± 3	305 ± 4	−4 ± 1%
South	320 ± 4	316.7 ± 0.6	−1 ± 1%
South West	317 ± 3	307 ±6	−3 ± 2%
West	325 ± 6	302 ± 3	−7 ± 2%
North West	333.2 ± 0.4	279 ± 4	−16 ± 1%
Centre	289.6 ± 0.5	263 ± 2	−9 ± 1%

Table A.4: Average DLP in CTDI body phantom for a standard GE scan and a scan with ODM. The values are the average of three measurements ± one standard deviation, reported with one significant digit in the standard deviation. The relative change shows the difference between the standard and ODM scans. *) Value based on only two measurements due to a scanning error.

Position	DLP standard scan [mGy·cm]	DLP ODM [mGy·cm]	Relative change
North	51.9 ± 0.2	32.6 ± 0.4*	−37 ± 1%
North East	51.7 ± 0.9	34.1 ± 0.3	−34 ± 1%
East	51.92 ± 0.05	43.63 ± 0.09	−16.0 ± 0.2%
South East	40.93 ± 0.07	39.7 ± 0.2	−3 ± 1%
South	41.0 ± 0.1	40 ± 2	−3 ± 4%
South West	40 ± 1	39 ± 1	−5 ± 4%
West	51.9 ± 0.8	43 ± 1	−18 ± 2%
North West	51 ± 2	34.2 ± 0.3	−33 ± 2%
Centre	21.71 ± 0.06	17.6 ± 0.2	−19 ± 1%

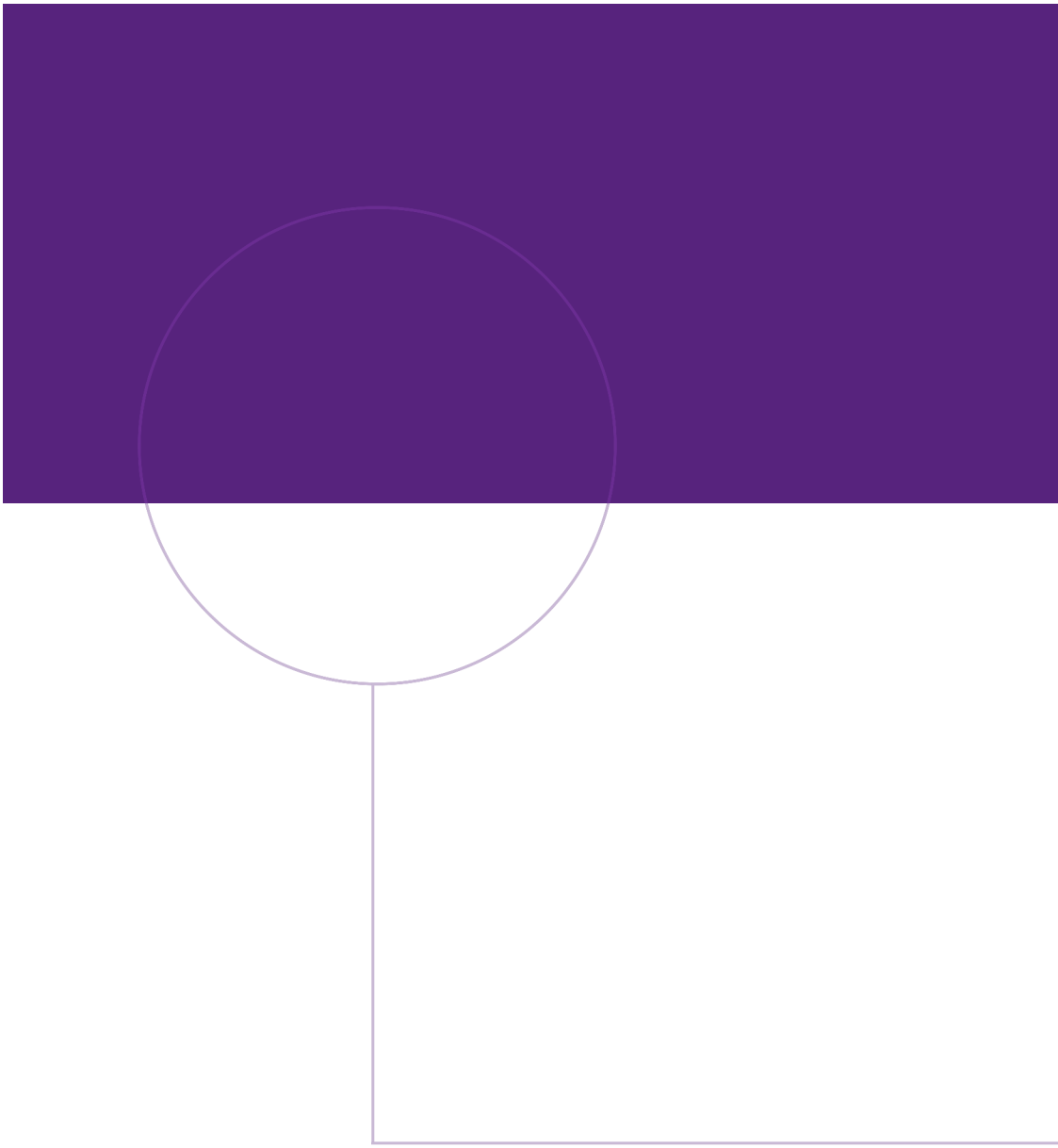

NTNU

Kunnskap for ei betre verd